PCCP

A Combined Crossed Molecular Beams and Computational Study on the Formation of Distinct Resonantly Stabilized C_5H_3 Radicals via Chemically Activated C_5H_4 and C_6H_6 Intermediates

Journal:	*Physical Chemistry Chemical Physics*
Manuscript ID	CP-ART-01-2018-000357.R2
Article Type:	Paper
Date Submitted by the Author:	07-Mar-2018

Complete List of Authors:	Thomas, Aaron; University of Hawaii, Chemistry Lucas, Michael; University of Hawaii, Chemistry Zhao, Long; University of Hawaii at Manoa, Department of Chemistry Liddiard, Jerid; University of Hawaii Kaiser, Ralf I; University of Hawaii, Mebel, Alexander; Florida International University, Chemistry and Biochemistry

A Combined Crossed Molecular Beams and Computational Study on the Formation of Distinct Resonantly Stabilized C_5H_3 Radicals via Chemically Activated C_5H_4 and C_6H_6 Intermediates

Aaron M. Thomas, Michael Lucas, Long Zhao, Jerid Liddiard, Ralf I. Kaiser*

Department of Chemistry, University of Hawai'i at Mānoa, Honolulu, HI 96822, United States

Alexander M. Mebel*

Department of Chemistry and Biochemistry, Florida International University, Miami, FL 33199, United States

ABSTRACT

The crossed molecular beams technique was utilized to explore the formation of three isomers of resonantly stabilized (C_5H_3) radicals along with their d_2-substituted counterparts via the bimolecular reactions of singlet/triplet dicarbon [$C_2(X^1\Sigma_g^+/a^3\Pi_u)$] with methylacetylene [$CH_3CCH(X^1A_1)$], d_3-methylacetylene [$CD_3CCH(X^1A_1)$], and 1-butyne [$C_2H_5CCH(X^1A')$] at collision energies up to 26 kJ mol^{-1} via chemically activated singlet/triplet C_5H_4/C_5D_3H and C_6H_6 intermediates. These studies exploit a newly developed supersonic dicarbon [$C_2(X^1\Sigma_g^+/a^3\Pi_u)$] beam generated via photolysis of tetrachloroethylene [$C_2Cl_4(X^1A_g)$] by excluding interference from carbon atoms, which represent the dominating (interfering) species in ablation-based dicarbon sources. We evaluated the performance of the dicarbon [$C_2(X^1\Sigma_g^+/a^3\Pi_u)$] beam in reactions with methylacetylene [$CH_3CCH(X^1A_1)$] and d_3-methylacetylene [$CD_3CCH(X^1A_1)$]; the investigations demonstrate that the reaction dynamics match previous studies in our laboratory utilizing ablation-based dicarbon sources involving the synthesis of 1,4-pentadiynyl-3 [$HCCCHCCH(X^2B_1)$] and 2,4-pentadiynyl-1 [$H_2CCCCCH(X^2B_1)$] radicals via hydrogen (deuterium) atom elimination. Considering the $C_2(X^1\Sigma_g^+/a^3\Pi_u)$ - 1-butyne [$C_2H_5CCH(X^1A')$] reaction, the hitherto elusive methyl-loss pathway was detected. This channel forms the previously unknown resonantly stabilized penta-1-yn-3,4-dienyl-1 [$H_2CCCHCC(X^2A)$] radical along with the methyl radical [$CH_3(X^2A_2'')$] and is open exclusively on the triplet surface with an overall reaction energy of −86 ± 10 kJ mol^{-1}. The preferred reaction pathways proceed first by barrierless addition of triplet dicarbon to the π-electronic system of 1-butyne, either to both acetylenic carbon atoms or to the sterically more accessible carbon atom, to form the methyl-bearing triplet C_6H_6 intermediates [**i4$_{1b}$**] and [**i8$_{1b}$**], respectively, with the latter decomposing via a tight exit transition state to penta-1-yn-3,4-dienyl-1 [$(H_2CCCHCC(X^2A)$] plus the methyl radical [$CH_3(X^2A_2'')$]. The successful unraveling of this methyl-loss channel – through collaborative experimental and computational efforts – underscores the viability of the photolytically generated dicarbon beam as an unprecedented tool to access reaction dynamics underlying the formation of resonantly stabilized free radicals (RSFR) that are vital to molecular mass growth processes that ultimately lead to polycyclic aromatic hydrocarbons (PAHs).

1. Introduction

During the last decades, reactions of the dicarbon molecule (C_2), which has been detected in combustion flames,[1-3] cometary comae,[4,5] and in the interstellar medium (ISM),[6,7] with unsaturated hydrocarbons have received considerable attention due to its role as a key reactant in gas phase molecular growth processes. These can lead to polyynes ($C_{2n}H_2$) along with their radicals ($C_{2n}H$), resonantly stabilized free radicals (RSFRs), and ultimately to polycyclic aromatic hydrocarbons (PAHs) through the production of open shell reaction intermediates formed via bimolecular collisions characterized by barrierless entrance channels and overall exoergic pathways. Strong transitions from its electronic ground $X^1\Sigma_g^+$ and first excited $a^3\Pi_u$ states have made dicarbon a tracer for determining chemical rate constants,[8] measuring stellar temperatures and composition,[9-11] and unraveling the molecular complexity of macrostructures like cold clouds[12] and protoplanetary nebulae.[13,14] Consequently, the formation,[15-17] structure,[18-20] and reactivity[21-23] of dicarbon remains of broad interest as evidenced by the continued expansion of the kinetics and chemical dynamics underscoring dicarbon reactivity.

More specifically, dicarbon is instrumental in the growth of polyynes ($C_{2n}H_2$) and their radicals through addition mechanisms via the $C_2 + C_{2n}H_2 \rightarrow C_{2n+2}H + H$ reaction sequence.[24-30] These reactions are barrier-less and proceed via addition of dicarbon to the acetylenic π electrons. Singlet dicarbon adds to the carbon-carbon triple bond of $C_{2n}H_2$ forming first a tricyclic reaction intermediate $[C_{2n+2}H_2]^*$ that then isomerizes to a linear $HC_{2n+2}H$ global minimum before dissociation via elimination of a hydrogen atom to form the $C_{2n+2}H$ radical. On the other hand, the addition of triplet dicarbon to $C_{2n}H_2$ is more complex as it can occur at a single carbon atom or to both carbon atoms of the acetylenic moiety (C≡C) simultaneously – as in the singlet case – followed by isomerization and cleavage of the carbon-carbon bond in dicarbon. The experimental chemistry of dicarbon reactions with (poly)acetylenes has culminated in the synthesis of key polyethynyls: butadiynyl (C_4H),[24-28] hexatriynyl (C_6H),[29] and octatetranyl (C_8H) (Scheme 1).[30] These radicals undergo exoergic reactions with acetylene to form $C_{2n+2}H_2$ alongside atomic hydrogen;[31] this furthers the chain elongation initiated by dicarbon. Notably, the spectroscopic signatures for dicarbon along with the aforementioned polyethynyls and their relevant (poly)acetylene precursors [acetylene (HCCH), diacetylene

(HCCCCH), triacetylene (HCCCCCCH)] have been identified in circumstellar envelopes of the dying carbon star IRC+10216 and also in cold molecular clouds.[32-39]

Further, resonantly stabilized free radicals (RSFRs) – relatively long lived open shell transient molecules with added stability due to electron delocalization – can be formed in hydrogen exchange reactions with carbon[40-43] and dicarbon,[44-48] or as reactive intermediates from their radical hydrides methylidyne (CH)[49-51] and ethynyl (C_2H).[52-55] The propargyl (H_2CCCH, IV) abundance is suggested to be strongly correlated with the formation of the simplest aromatic systems benzene (C_6H_6) and phenyl (C_6H_5, XI) (Scheme 1).[56] Oxidation of phenyl radicals yields cyclopentadienyl (c-C_5H_5),[57] which may initiate naphthalene ($C_{10}H_8$) formation via the self-reaction $C_5H_5 + C_5H_5 \rightarrow C_{10}H_8 + 2H$.[58,59] The conversion of naphthyl ($C_{10}H_7$) to indenyl (C_9H_7) through oxidation is analogous to the aforementioned $C_6H_5O_2 \rightarrow C_5H_5 + O + CO$ pathway with the resulting C_9H_7 radicals suggested to react with propargyl (C_3H_3) and cyclopentadienyl (c-C_5H_5) to ultimately form PAHs acenaphthylene[56] ($C_{12}H_8$) and phenanthrene ($C_{14}H_{10}$),[60] respectively. Hence resonantly stabilized free radicals are critical for mass-growth processes leading to PAHs. In this context, the C_5H_3 isomers have garnered considerable interest due to their presence in benzene flames.[61-63] The global minimum is a resonantly stabilized propargyl derivative, *i*-C_5H_3 ($H_2CCCCCH$), that has also been observed in allene, methylacetylene, and cyclopentene (c-C_5H_8) flames.[63] C_5H_3 radicals therefore have been explored in PAH formation networks.[64,65]

The $H_2CCCCCH$ radical (Scheme 1, V) has been synthesized under single collision conditions in bimolecular reactions of dicarbon with methylacetylene (CH_3CCH)[66] and allene (H_2CCCH_2)[67] and is predicted to be a methyl-loss product of dicarbon reactions with three C_4H_6 isomers (Scheme 1): 1,2-butadiene ($H_2CCCHCH_3$), 1-butyne (C_2H_5CCH), and dimethylacetylene (CH_3CCCH_3).[68] Under single-collision conditions afforded by crossed molecular beams (CMB) experiments, several radicals,[24-30,69,70] including resonantly stabilized[44-48,71] and aromatic[48,72-75] varieties, have been produced in dicarbon reactions with closed shell reaction partners. Despite these successes, hydrocarbons produced via methyl-loss channels have remained elusive. In a recent CMB study of dicarbon with 1-butyne (C_2H_5CCH),[68] in which dicarbon was produced alongside atomic carbon and tricarbon (C_3) using a versatile ablation source,[76-81] only those reactions leading to C_6H_5 isomers could be observed. Any $[C_6H_6]^*$ dissociations leading to methyl-loss channels were obscured by products of the simultaneous reaction of carbon[82] with

any C_4H_6 isomer leading to C_5H_5 plus atomic hydrogen.[83-85] Here, upon ionization and fragmentation by electron impact (80 eV), the $C_5H_5^+$ molecular ion fragments to $C_5H_4^+$, $C_5H_3^+$, and smaller species thus masking the C_5H_3 product in the unimolecular decomposition of any $[C_6H_6]^*$ intermediate via the methyl-loss pathway. Furthermore, the number density of products N reaching the detector is defined as $N(\Theta, v) = I_{CM}(\theta, u)\, v\, u^{-2}$ with the velocities u and v and scattering angles θ and Θ of the product in the laboratory and center-of-mass (CM) reference frames, respectively, and $I_{CM}(\theta, u)$ is the CM reactive differential cross-section.[86] For a unimolecular decomposition, the velocity of the heavy product is proportional to the mass of the light product, i.e. C_5H_5 formed in the atomic carbon reaction ($[C_5H_6]^* \rightarrow C_5H_5 + H$) will carry a smaller velocity than the C_5H_3 formed in the dicarbon system ($[C_6H_6]^* \rightarrow C_5H_3 + CH_3$). Considering the effects of dissociative ionization, methyl-loss channels of dicarbon reactions are not likely observable using electron impact ionization, if a simultaneous atomic carbon reaction is ongoing (Figure 1) in particular since the concentration of carbon is typically one order of magnitude higher than the dicarbon concentration.

Considering the complication of currently operating dicarbon ablation and discharge sources in molecular beams machines, a new source design is clearly needed to access potential methyl-loss channels. Here, we present a novel supersonic source of dicarbon produced via photodissociation of tetrachloroethylene (C_2Cl_4). While tetrachloroethylene (C_2Cl_4) has long been exploited as a dicarbon precursor in kinetic assessments,[87-94] it has not been introduced as a dicarbon source in CMB experiments which have thus far relied on graphite ablation,[76,95] electrical (DC)[96] or radio-frequency (RF)[97] discharge into gaseous carbon-bearing precursors for dicarbon production. Photolysis (248 nm) of a tetrachloroethylene – helium mixture yields ground and electronically excited dicarbon with no interference from atomic carbon or tricarbon making it a valuable tool for fully exploring dicarbon reaction pathways that would otherwise be obscured by reactive scattering originating from reactive carbon atoms. The performance of this source is tested for the well-characterized methylacetylene – dicarbon[66,98-100] and d_3-methylacetylene – dicarbon systems[101] before demonstrating its potential for the detection of the hitherto elusive methyl-loss channel in the dicarbon – 1-butyne (C_2H_5CCH) system.

2. Experimental and Calculation Methods

2.1. Experiment

The dicarbon (C_2; $X^1\Sigma_g^+/a^3\Pi_u$) reactions with methylacetylene (CH_3CCH; X^1A_1), d_3-methylacetylene (CD_3CCH; X^1A_1), and 1-butyne (C_2H_5CCH; X^1A') were conducted under single-collision conditions using a crossed molecular beams (CMB) machine at the University of Hawaii.[49] The machine employs two orthogonal fixed molecular beam sources and a detector that is rotatable in the plane defined by both reactant beams. The detector comprises a Brink-type ionizer,[102] quadrupole mass spectrometer (QMS), and a Daly-type ion counter.[103] Subdivided into three regions, differential pumping of the detector reduces operating pressures to less than 10^{-11} Torr in the inner most section that houses the ionizer. Products of the reactive scattering process in the dicarbon reactions with methylacetylene (Organic Technologies, 99%+), d_3-methylacetylene (CDN Isotopes, 99%+), and 1-butyne (Aldrich Chemistry, ≥ 98%) were ionized by electron impact (40 eV; 1.4 mA) and filtered according to mass-to-charge (*m/z*) ratios using the QMS (Extrel; QC 150) equipped with a 2.1 MHz oscillator. The resulting ions were accelerated by a negative 22.5 kV potential onto an aluminum coated stainless-steel target, generating a cascade of secondary electrons directed toward an aluminum coated scintillator. The photoemission was collected by a photomultiplier tube (PMT, Burle, Model 8850) operated at a negative potential of 1.35 kV, whose output was discriminated at 1.6 mV (Advanced Research Instruments, Model F-100TD).

The data collection was coordinated by a four-slot (0.76 mm) chopper wheel rotating at 120 Hz equipped with an infrared photodiode that permits system-wide synchronization by acting as a time zero and trigger (T_0 = 0 μs) for the equipment discussed herein. The resulting 480 Hz signal was processed by an f/8 frequency divider and ultimately distributed amongst four Stanford Research Systems (SRS) DG535 delay/pulse generators (PDG I – IV). The +4 V, 50 Ω outputs AB ($A_I = T_0$ + 1888 μs, $B_I = A_I$ + 80 μs) & CD ($C_I = A_I$ − 50 μs, $D_I = C_I$ + 80 μs) of PDG I were fed into a homemade pulse shaper and then amplified by a power amplifier (Physik Instrumente, E-421). These 60 Hz signals were sent to the primary and secondary pulsed valves (Proch-Trickl),[104] each containing a piezoelectric disc translator (Physik Instrumente, P-286.23), resulting in 80 μs opening times using amplitudes of −360 V to −400 V for this set of experiments. PDG I A (TTL, high impedance) was halved to 30 Hz and delivered to PDGs II and III for further distribution. PDG II AB ($A_{II} = T_0$ + 1888 μs; $B_{II} = A_{II}$ + 5 μs) was used to trigger a SRS 430 multichannel scaler (MCS). PDG III output CD ($C_{III} = T_0$ + 2048 μs; $D_{III} = C_{III}$ + 15 μs; TTL; 50 Ω) was sent to an excimer laser (Coherent: Compex110, 120 mJ/pulse), while PDG III

A (TTL high impedance) was divided by 3 and delivered to PDG IV, which provided 10 Hz TTL (50 Ω) signals to the flash lamp and Q-switch of a Quantel Brilliant Nd:YAG laser via outputs AB ($A_{IV} = T_0 + 1889$ μs, $B_{IV} = A_{IV} + 5$ μs) and CD ($C_{IV} = T_0 + 2075$ μs, $D_{IV} = C_{IV} + 5$ μs), respectively, used to pump a tunable dye laser (Lambda Physik Scanmate Pro). This synchronization scheme is compiled in Figure 2.

Dicarbon was produced by photodissociation of tetrachloroethylene (C_2Cl_4, Sigma Aldrich, ≥ 99.9 %), purified by multiple freeze-pump-thaw cycles and seeded in helium (99.9999 %; AirGas) at 2.2 atm in a room temperature (300 K) stainless steel bubbler. Photodissociation of the tetrachloroethylene in this gas mixture (1.4 % C_2Cl_4) was accomplished using 248 nm focused to 1.2 × 4.0 mm^2 approximately 1 mm downstream of the pulsed valve; the distance between the nozzle and the skimmer was optimized to 19 ± 1 mm. The resulting dicarbon molecules passed through a 1 mm skimmer before velocity-selection by the chopper wheel. On-axis (Θ = 0°) characterization of dicarbon at 34 eV electron energy reveals a high intensity beam (2.5 that achieved by graphite ablation) with a narrow velocity distribution, with peak velocities v_p ranging from 1567 to 1596 m s^{-1} and speed ratios S ranging from 9.6 to 12.0. The hydrocarbon reactants were expanded neat from a pulsed valve in the secondary source chamber and then skimmed before perpendicularly intersecting the dicarbon beam. Unlike the dicarbon beam, whose velocity was selected *in situ*, the velocity distributions of the hydrocarbon beams were characterized on axis (Θ = 90°) prior to reactive scattering experiments using a detector-mounted chopper wheel. For the dicarbon – methylacetylene [CH_3CCH (CD_3CCH)] reaction, the secondary pulsed valve was backed by 600 (500) Torr with v_p = 800 ± 10 (790 ± 10) m s^{-1} and S = 12.0 ± 0.4 (12.0 ± 0.4), resulting in a collision energy E_C of 23.2 ± 0.3 (24.0 ± 0.2) kJ mol^{-1} and a center-of-mass angle Θ_{CM} of 40.4 ± 0.4° (41.9 ± 0.4°). The heavier 1-butyne (C_2H_5CCH) (550 Torr) reactant intersects the dicarbon beam in the reaction center with v_p = 782 ± 14 m s^{-1} and S = 8.6 ± 0.5, and therefore E_C = 26.2 ± 0.8 kJ mol^{-1} and Θ_{CM} = 47.8 ± 0.7° for reactive collisions with dicarbon. The peak velocities v_p and speed ratios S, along with relevant collision energies E_C and center-of-mass angles Θ_{CM} for C_2, CH_3CCH, CD_3CCH, and C_2H_5CCH are tabulated in Table 1.

Angularly resolved time-of-flight (TOF) spectra were obtained in the plane of the reactant beams at laboratory angles 0° ≤ Θ ≤ 69° with respect to the dicarbon beam (Θ = 0°) and analyzed using a forward-convolution routine[105,106] that relies on user-defined center-of-mass (CM) frame

translational energy $P(E_T)$ and angular $T(\theta)$ flux distributions. Accounting for the reactant beam divergences, velocity spreads, and machine parameters, laboratory-frame TOF spectra and angular distributions (LAD) are calculated and compared with the experimental data. The $P(E_T)$ and $T(\theta)$ functions are varied iteratively until a best fit of the experimental dataset are obtained. These functions comprise the reactive differential cross section $I(\theta, u)$, which is taken to be separable into its CM scattering angle θ and CM velocity u components, $I(u, \theta) \sim P(u) \times T(\theta)$. The differential cross section is plotted as a flux contour map that serves as an image of the reaction. Errors of the $P(E_T)$ and $T(\theta)$ functions are determined within the 1σ error limits of the accompanying LAD while maintaining a good fit of the laboratory TOF spectra.

Molecular beams of dicarbon are known to contain both the singlet ground ($X^1\Sigma_g^+$) state and the lowest lying triplet state ($a^3\Pi_u$),[49,107] which are separated by only 7.3 kJ mol^{-1}.[108] While higher energy states may be products of the initial tetrachloroethylene photodissociation, the $b^3\Sigma_g^-(v=0)$ and $A^1\Pi_u(v=0)$ lifetimes are only 16.6 μs and 13.0 μs, respectively,[109] and less than the 29.2 ± 0.6 μs flight time of dicarbon to the reaction center. The rovibrational energy distributions of the ground and first excited states of dicarbon were characterized by laser induced fluorescence (LIF) using a tunable dye laser pumped by the third harmonic of an integrated Nd:YAG laser. Emissions from dicarbon were focused before passing an interference filter (Andover Corporation) centered at 230.40 nm (FWHM of 10.09 nm) or 561.20 nm (FWHM of 9.25 nm) mounted at the entrance window of a Hamamatsu R955 PMT. The ground state was probed using the Mulliken $D^1\Sigma_u^+ - X^1\Sigma_g^+$ (0,0) and (1,1) transitions. Tunable radiation near 231 nm (6 nJ pulse^{-1}) was obtained by frequency-doubling the fundamental output of the dye laser circulating Coumarin 460 (Exciton). The triplet state was accessed using the Swan $d^3\Pi_g \leftarrow a^3\Pi_u$ excitations near 512.5 nm (1,1) and 517.5 nm (0,0) using light obtained by circulating Coumarin 503 (Exciton) attenuated to 16 nJ/pulse. Fluorescence was captured on the $\Delta v = -1$ sequence near 563.5 (0,1) and 558.5 (1,2) nm. The LIF spectra were analyzed by comparison with spectral simulations obtained from PGOPHER[110] using spectroscopic constants for the $D^1\Sigma_u^+ - X^1\Sigma_g^+$ system from Schmidt and Baskay,[109] and from Brooke et al.[111] for the $d^3\Pi_g - a^3\Pi_u$ system. The LIF spectra of the Mulliken ($D^1\Sigma_u^+ - X^1\Sigma_g^+$) and Swan ($d^3\Pi_g - a^3\Pi_u$) bands are provided in Figure 3. A comparison with spectral simulations suggest the $X^1\Sigma_g^+(v=0)$ and $a^3\Pi_u(v=0)$ states are the most populated, each with a bimodal temperature representation as typified in radical beams.[49,112] The $X^1\Sigma_g^+(v=1)$ state lies 22 kJ mol^{-1} above $X^1\Sigma_g^+(v=0; j=0)$, with rotational

temperatures of 1,000 K contributing an additional 4 kJ mol^{-1}. Rotational temperatures of 300 K in the $a^3\Pi_u(v=1)$ state bring the energy to 26 kJ mol^{-1} above dicarbon's ground singlet state.[108] The relative vibrational populations and rotational temperatures for $X^1\Sigma_g^+$ and $a^3\Pi_u$ are compiled in Table 2.

2.2. Calculations

Stationary points on the triplet C_6H_6 potential energy surfaces (PES) accessed by the $C_2(a^3\Pi_u)$ + 1-butyne reaction, which were not considered in the previous work, were calculated at the same level of theory as earlier.[68] In particular, geometries of all structures were optimized and vibrational frequencies were computed at the hybrid density functional B3LYP/6-311G** level of theory.[113,114] Energies of various species were refined using the coupled cluster CCSD(T) method[115] with Dunning's correlation-consistent cc-pVDZ, cc-pVTZ, and cc-pVQZ basis sets[116] and then the total energies were extended to the complete basis set (CBS) limit using either two-point (CBS(dt)) or three-point (CBS(dtq)) extrapolation.[68,117] For the $C_2(a^3\Pi_u)$ + methylacetylene system, extrapolation to the CBS limit was achieved via explicitly correlated CCSD(T)-F12 calculations[118,119] with the cc-pVTZ-f12 basis set. The B3LYP and CCSD(T) quantum chemical calculations were performed using the GAUSSIAN 09[120] and MOLPRO 2010[121] program packages. Rate constants of all unimolecular reaction steps on the triplet C_6H_6 PES following initial association of $C_2(a^3\Pi_u)$ with 1-butyne were computed using Rice-Ramsperger-Kassel-Marcus (RRKM) theory,[122-124] as functions of available internal energy of each intermediate or transition state, where numbers and densities of states were obtained within the harmonic approximation using B3LYP/6-311G** computed frequencies. The internal energy was taken as a sum of the collision energy and a negative of the relative energy of a species with respect to the reactants (the chemical activation energy). One energy level was considered throughout as at a zero pressure limit. Then, RRKM rate constants were utilized to compute product branching ratios by solving first-order kinetic equations within steady-state approximation. More detail on the ab initio/RRKM calculations can be found in the previous publication.[68]

3. Results

3.1. Laboratory Data

3.1.1. Dicarbon - Methylacetylene

Dicarbon (C_2; 24 amu) reacted with methylacetylene (CH_3CCH; 40 amu) with an average collision energy E_C of 23.2 ± 0.3 kJ mol^{-1}. We monitored potential reaction products at mass-to-charge ratios (*m/z*) 64 ($C_5H_4^+$), 63 ($C_5H_3^+$), 62 ($C_5H_2^+$), and 49 (C_4H^+) and were able to collect a TOF at each mass except for *m/z* 49 , at which no signal was detected. The TOF signal at *m/z* 64 ($C_5H_4^+$) and 62 ($C_5H_2^+$) are superimposable with *m/z* 63 ($C_5H_3^+$) after scaling, and hence $C_5H_2^+$ derives from fragmentation of $C_5H_3^+$ in the ionizer, whereas the signal at *m/z* 64 is attributable to $^{13}CC_4H_3^+$. Accordingly, TOFs were recorded at *m/z* 63 in 2.5° steps from 8.5° to 67.5° (Figure 4). The laboratory angular distribution (LAD) of $C_5H_3^+$, which contains information from 2.1×10^6 TOF spectra, is plotted as a function of the laboratory angle (Θ) in Figure 5 as black dots with 1σ error bars. It is clear that the distribution has two distinct contributions from the two maxima in the total distribution occurring at 20° and 40°. The LAD maximum at 40.0° falls within 1σ of the Θ_{CM} for dicarbon-methylacetylene reactive scattering. The second channel peaking at Θ = 20° can only be fit with the mass combination of the chloroethynyl radical (C_2Cl, $X^2\Pi$) – a byproduct of the tetrachloroethylene photodissociation leading to $C_2{}^{35}Cl$ (59 amu) and $C_2{}^{37}Cl$ (61 amu) [125] – with methylacetylene (C_3H_4; 40 amu). The center-of-mass angle Θ_{CM} of this system is 19.6 ± 0.3°, close to the distribution maximum of this channel. The LAD taken at *m/z* 63 is thus split into two components owing to scattering of dicarbon (C_2) and chloroethynyl (C_2Cl) with the hydrocarbon as shown as red and blue curves, respectively (Figure 5). For Θ < 25° the data are best fit with the reaction $C_2{}^{35}Cl + CH_3CCH$ leading to atomic chlorine and/or hydrogen chloride products. The imposing product signal from reactive scattering of C_2 + CH_3CCH limits our ability to reasonably constrain this channel, and we find that acceptable fits of the total signal obtained at *m/z* 63 can be obtained with either a Cl or HCl loss. The center-of-mass functions for the HCl loss channel, used to fit the C_2Cl contribution to the reactive scattering signal recorded at *m/z* 63, depict a slightly backward distribution and suggest a reaction energy of about 13 ± 3 kJ mol^{-1} (Figure S1). A full investigation of the C_5H_4Cl potential energy surface is beyond the scope of this paper and therefore the remainder of our discussion will focus on the reactivity of dicarbon. For Θ > 25°, ion counts from the $C_2 + CH_3CCH \rightarrow C_5H_3 + H$ reaction dominate the LAD, with C_5H_3 products being spread from 17.5° to 62.5° in the laboratory frame. In this regime the TOFs and LAD could be fit with a single channel, namely C_2 (24 amu) + CH_3CCH (40 amu) → C_5H_3 (63 amu) + H (1 amu), resulting in a nearly symmetric distribution about the maximum at 40°.

3.1.2. Dicarbon – d_3-Methylacetylene

The dicarbon (C_2; 24 amu) reaction with d_3-methylacetylene (CD_3CCH; 43 amu) was carried out at a collision energy E_C = 24.0 ± 0.2 kJ mol^{-1}. Reactive scattering products were monitored at *m/z* 66 ($C_5D_3^+$) and 65 ($C_5HD_2^+$) along Θ_{CM} = 41.9 ± 0.4° to discriminate if the aforementioned atomic hydrogen loss originated from the methyl group (here: CD_3) or from the acetylenic moiety. Ion signal was observed at both *m/z* 66 and *m/z* 65. The signal at *m/z* 66 is much weaker than *m/z* 65 and is superimposable with *m/z* 65 after scaling. Signal at *m/z* 65 cannot derive from fragmentation of $C_5D_3^+$ (*m/z* 66) since the latter can only fragment via deuterium loss to $C_5D_2^+$ (*m/z* 64). Since no adduct was detected, the signal recorded at *m/z* 65 is attributed to $C_5HD_2^+$, whereas that observed at *m/z* 66 must originate from $^{13}CC_4HD_2^+$. Therefore, TOF spectra were collected at *m/z* 65 from 11° to 66° in 5° steps (Figure 6). The broadening of the LAD at $\Theta < 30°$ is due to scattering of the d_3-methylacetylene reactant with chloroethynyl (C_2Cl) as seen in the analogous dicarbon – methylacetylene system discussed above. Considering the decreased signal-to-noise (C_5HD_2 analysis derives from about 5.3×10^5 TOF spectra), contributions from chloroethynyl are more difficult to resolve in the TOF spectra. Accounting for the chloroethynyl contributions to the *m/z* 65 signal, the dicarbon component could be fit with a single channel, $C_2 + CD_3CCH \rightarrow C_5HD_2$ (65 amu) + D (2 amu). The C_5HD_2 signal is confined to a spread of about 55° in the laboratory frame and is nearly symmetric about Θ_{CM} (red curve, Figure 7).

3.1.3. Dicarbon – 1-Butyne

Finally, the products of the dicarbon (C_2; 24 amu) plus 1-butyne (C_2H_5CCH; 54 amu) reaction were monitored at *m/z* 78 ($C_6H_6^+$), 77 ($C_6H_5^+$), 76 ($C_6H_4^+$), and 63 ($C_5H_3^+$). Scattering signals were observed along Θ_{CM} = 47.8 ± 0.7° at *m/z* 77, 76 and 63. The superimposability of the *m/z* 76 and *m/z* 77 TOF spectra indicate that each arise from $C_6H_5^+$, with $C_6H_5^+$ fragmenting upon ionization of the neutral product to $C_6H_4^+$. The $C_2 + C_2H_5CCH \rightarrow C_6H_5 + H$ reaction was previously interrogated in a combined experimental and computational study;[68] an examination of this channel is not repeated here. Regarding the signal at *m/z* 63, we collected 1.4×10^7 TOF

spectra (Figure 8) in 10° steps from 18° to 68° (Figure 9). A fast feature is apparent in TOF spectra at $\Theta \leq 28°$. Unlike the C_2 + CH_3CCH/CD_3CCH reactions that were accompanied by a reactive chloroethynyl partner, the magnitude of this signal increases monotonically toward the dicarbon beam and is thus attributed to nonreactive scattering of the C_2Cl_4 precursor – a phenomenon in radical beam sources at angles close to the primary beam.[126] Considering the methyl co-fragment, the heavy C_5H_3 product scatters broadly in our CMB and extends well beyond the angular limitations of our apparatus.

3.2. Center-of-Mass Functions

The center-of-mass functions hold important information and assist in the elucidation of the underlying reaction dynamics (Figures 10-12). For the C_2 - CH_3CCH system, the *T(θ)* of the atomic hydrogen loss channel forming C_5H_3 isomers exhibits intensity at all angles, but slightly favors intensity in the forward hemisphere with respect to the dicarbon beam ($\theta = 0°$) with a forward-backward ratio at the poles of *T(0°)/T(180°)* = 1.5 ± 0.4 (Figure 10, *T(θ)*). This distribution suggests indirect scattering dynamics[127] and the existence of a $[C_5H_4]^*$ intermediate(s) possessing a mean lifetime τ approximately twice of its rotational period τ_r, where τ is given by $\log_e(T(0°)/\ T(180°))^2)^{-1}\tau_r$.[128] The corresponding translational energy flux distribution $P(E_T)$ extends out to a maximum translational energy E_{max} of 204 ± 24 kJ mol^{-1}. Considering that the maximum available energy for translation (E_{max}) represents the sum of the absolute of the reaction energy ($\Delta_r G$) plus the collision energy (E_C), the best fitting indicated a reaction energy of −181 ± 25 kJ mol^{-1}. The derived reaction energy can be reduced by up to 26 kJ mol^{-1} for reactions with singlet dicarbon, or by up to 28 kJ mol^{-1} for those involving triplet dicarbon ($a^3\Pi_u$) when accounting for the rovibrational distribution of our beam (LIF section of *Experimental Methods*). The best fitting $P(E_T)$ peaks near 19 kJ mol^{-1}, although the experimental data could be fit reasonably well with a plateau-like maximum that ranges from 3 to 23 kJ mol^{-1} (Figure 10, $P(E_T)$). This broad feature suggests that C_5H_3 formation occurs through multiple exit transition states.[98] This peaking of the $P(E_T)$ at low translational energies suggests that C_5H_3 formation occurs through relatively loose exit transition state(s). Moreover, the average translational energy $\langle E_T \rangle$ of 50 ± 6 kJ mol^{-1} reveals that only 25 ± 4% of the available energy is

deposited into translational degrees of freedom. The latter suggests the reaction pathway is indirect.

For the C_2 - CD_3CCH reaction, the *T(θ)* of C_5HD_2 formed by atomic deuterium loss is also weakly polarized peaking in the forward direction (*T(0°)/T(180°)* = 1.1 ± 0.1) with intensity at all angles (Figure 11, *T(θ)*). This CM angular flux distribution suggests indirect reaction dynamics as well involving one or more C_5HD_3 isomers with an average lifetime of about 2.7 τ_r. The translational energy flux distribution $P(E_T)$ could be fit with a high energy cutoff in the region $153 \leq E_{max} \leq 219$ kJ mol^{-1} (Figure 11, $P(E_T)$). The best fit corresponds to E_{max} = 193 kJ mol^{-1} which gives a derived reaction energy of −169 ± 25 kJ mol^{-1} for the deuterium atom loss channel. The best fitting $P(E_T)$ peaks near 13 kJ mol^{-1}, but the data could also be fit with a broad distribution maximum ranging from 5 to 16 kJ mol^{-1}. Once more, the latter suggests that C_5HD_2 formation involves at least two dissociation channels. This $P(E_T)$ also indicates that on average 24 ± 6% of the available energy is disposed into translation, further suggesting contributions from an indirect reaction mechanism as noted in *T(θ)*.

In the C_2 - C_2H_5CCH system the CM angular flux distribution of the methyl (CH_3) elimination channel exhibits intensity across all angles (Figure 12, *T(θ)*). This *T(θ)* is slightly backward scattered with respect to dicarbon, with *T(0°)/T(180°)* = 0.9 ± 0.1. Furthermore, the *T(θ)* dips near θ = 63°. This suggests that at least one exit channel involves the methyl-loss within the rotational plane of the dissociating $[C_6H_6]^*$ complex due to efficient coupling of orbital angular momentum between the reactant and product. The translational energy flux distribution (Figure 12, $P(E_T)$) for C_5H_3 formation extends out to E_{max} = 118 ± 16 kJ mol^{-1}, from which we obtain a reaction energy of −92 ± 16 kJ mol^{-1}. The most probable E_T is 15 ± 2 kJ mol^{-1} indicating a loose, product like transition state(s) leading to C_5H_3 plus CH_3. The average translational energy $\langle E_T \rangle$ of 32 ± 4 kJ mol^{-1} derived from $P(E_T)$ reveals that only 27 ± 5% channels into translational energy. Accordingly, at least one reaction channel leading to the C_5H_3 product isomers is indirect. Velocity vector (Newton) diagrams relating the laboratory and CM observations of C_5H_3 along with flux contour maps of the derived reactive differential cross section for each of the dicarbon reactions are compiled in Figures 13 and 14.

4. Discussion

In each of the three dicarbon reactions – C_2 + CH_3CCH, C_2 + CD_3CCH, and C_2 + C_2H_5CCH – we observed ions at *m/z* 63 (65) with time-of-flight (TOF) profiles indicative of C_5H_3 (C_5HD_2) formation in overall exoergic reactions. Recall that our dicarbon beam contains both $C_2(X^1\Sigma_g^+)$ and $C_2(a^3\Pi_u)$ reactants with v=0 states that differ by 7.3 kJ mol^{-1}. In discussing the results of our experiment, we leverage electronic structure calculations to determine which isomers represent the products formed in our experiments and to expose the underlying reaction mechanism governing their formation. This section is presented in two parts. The first part deals with the dicarbon-methylacetylene / d3-methylacetylene system demonstrating that – in comparison with previous studies on this system[66,67,98] – our new dicarbon source can be exploited for reactive scattering experiments. The second part elucidates a newly observed methyl-loss channel from a C_6H_6 reaction intermediate formed in the dicarbon plus 1-butyne system that was previously obscured due to complications arising from the ablation-sourced dicarbon beam and interference from reactions of carbon atoms.[68]

4.1. Dicarbon – (d_3)-Methylacetylene

To facilitate discussion of the dicarbon plus methylacetylene reaction we first consider the relevant C_5H_4 potential energy surface relating those bimolecular reactions of triplet ($a^3\Pi_u$) and singlet ($X^1\Sigma_g^+$) dicarbon with methylacetylene (X^1A_1) via C_5H_4 intermediates to dissociation product channels via atomic and/or molecular elimination. The singlet and triplet potential energy surfaces have been established by Mebel et al.[99] and by Gu et. al,[101] respectively, and have been reproduced in Figures 15 and 16. The triplet surface has been extended to include methyl-loss pathways that were not previously considered (Figure 16, red). Let us begin with events as they unfold on the singlet surface. Dicarbon in its singlet ground state can add without an entrance barrier either with its terminal end to the methylacetylene triple bond forming intermediate [**s1**] (CH_3CC_2CH), or across the triple bond to form a disubstituted tetracarbon ring [**s2**] (CH_3C_4H). All routes to dissociation products include the methyldiacetylene (CH_3CCCCH) global minimum, intermediate [**s3**], that lies 576 kJ mol^{-1} below the bimolecular entrance channel, and from which four new pathways emerge. Cleavage of the C−CH_3 bond leads to the

butadiynyl [$C_4H(^2\Sigma^+)$] (**p3$_{MA}$**) plus methyl (CH_3) product pair lying 20 kJ mol^{-1} below the separated reactants. Hydrogen loss can occur either from the acetylene end of [**s3**] (≡C−**H**) to form the methylbutadiynyl radical (CH_3CCCC; **p4$_{MA}$**), or from the [**s3**] methyl group (CH_2−**H**) to form the resonantly stabilized 2,4-pentadiynyl-1 (**p2$_{MA}$**) [$H_2CCCCCH(X^2B_1)$] radical in overall exoergic reactions. The **p4$_{MA}$** + H and **p2$_{MA}$** + H products lie 39 kJ mol^{-1} and 192 kJ mol^{-}1, respectively, below $C_2(X^1\Sigma_g^+)$ + $CH_3CCH(X^1A_1)$. Lastly, successive hydrogen migration from the [**s3**] methyl group via [**s4**] ultimately accesses the 1,4-pendiynyl-3 product isomer via hydrogen atom emission from [**s5**]. Intermediate [**s3**] isomerizes to the planar [**s4**] ($CH_2CHCCCH$) by hydrogen migration from the methyl group. Hydrogen atom loss from [**s4**] yields **p2$_{MA}$**, while isomerization from [**s4**] to [**s5**] ($CH_2CCHCCH$) via hydrogen shift eventually results in elimination of atomic hydrogen from the [**s5**] central carbon to form **p2$_{MA}$**, or from the [**s5**] methylene group to form 1,4-pentadiynyl-3 (**p1$_{MA}$**) [$HCCCHCCH(X^2B_1)$] with an overall reaction energy of −191 kJ mol^{-1}.

On the triplet surface three pathways are possible from the initial attack of dicarbon at the methylacetylene triple bond (Figure 16). Addition across the triple bond is barrierless and forms a tricarbon ring [**t1**] (CH_3CC_2CH) at the attack site that lies 170 kJ mol^{-1} below the separated reactants. Acyclic isomers of C_5H_4 are also possible via the barrierless addition of dicarbon to the terminal acetylenic carbon atom forming *trans* [**t2**] or *cis* [**t3**] pent-1-yn-3-en-diyl-1,4 (CH_3CCHC_2) radical intermediates. The cyclic [**t1**] can dissociate by methyl emission in an overall endoergic reaction (61 kJ mol^{-1}) via a loose transition state forming **p13$_{MA}$** (C_4H). [**t1**] can isomerize to [**t2**] by cleaving the C−C bond over a 53 kJ mol^{-1} barrier, or to an exotic rhomboid [**t4**] (CH_3C_4H) bicycle by ring closure to the methyl-bearing carbon atom in [**t1**], from which loss of the methyl group forms the bicyclic c-C_4H (**p12$_{MA}$**) product in an overall endoergic reaction (16 kJ mol^{-1}). Intermediate [**t4**] could also proceed to the disubstituted tricarbon ring [**t5**] (CH_3C_3CH) by ring opening via a 109 kJ mol^{-1} barrier. [**t5**] can undergo further ring opening by cleavage of the C−C bond joining the substituted carbon atoms producing a 5-carbon backbone [**t6**] (*trans*-CH_3CCCCH) with methyl and hydrogen termini. The exoergic butadiynyl (C_4H) plus methyl (CH_3) product channel is accessible from [**t6**] through loss of its methyl group and has an overall reaction energy of −70 kJ mol^{-1}. [**t6**] can also isomerize to [**t7**] (*cis*-CH_3CCCCH) via a low-lying barrier of 11 kJ mol^{-1}, from which follows atomic hydrogen loss

from the methyl substituent to yield the 2,4-pentadiynyl-1 ($H_2CCCCCH$) radical (**p2$_{MA}$**) in an overall exoergic reaction (−201 kJ mol^{-1}). Hydrogen loss from [**t2**] at the central carbon might form the methylbutadiynyl radical [$CH_3CCCC(X^2A_1)$], **p4$_{MA}$**, with an overall reaction exoergicity of −48 kJ mol^{-1}. Alternatively, [**t2**] can isomerize to the slightly more stable [**t3**] structure by traversing a relatively small barrier of 23 kJ mol^{-1}. From [**t3**] the system can pass through a 136 kJ mol^{-1} barrier via long range hydrogen migration, i.e. from the terminal methyl group to the terminal carbon atom of the dicarbon moiety resulting in an ethynyl-substituted propargyl-like system [**t8**] (CH_2CCHC_2H) that is stabilized by 366 kJ mol^{-1} relative to the separated reactants. Loose exit transition states from intermediate [**t8**] yield the C_5H_3 radicals 1,4-pentadiynyl-3 (**p1$_{MA}$**) and 2,4-pentadiynyl-1 and (**p2$_{MA}$**) via atomic hydrogen loss. The **p1$_{MA}$** + H and **p2$_{MA}$** + H product channels are overall exoergic by 200 and 201 kJ mol^{-1}, respectively.

Through consideration of our experimental results with the preceding discussion of the dicarbon-methylacetylene potential energy surface we can postulate the reaction mechanism(s) underlying the formation of C_5H_3 in our crossed molecular beams experiment. Recall that our derived reaction energy forming the C_5H_3 product isomer(s) plus atomic hydrogen is −181 ± 25 kJ mol^{-1} and agrees well with predicted reaction energies of the atomic hydrogen loss product channels leading to the 2,4-pentadiynyl-1 ($H_2CCCCCH$) and 1,4-pentadiynyl-3 (HCCCHCCH) radicals on the singlet and triplet potential energy surfaces,[101] and that the CM flux distributions reveal that the reaction proceeds through at least one $[C_5H_4]^*$ intermediate as indicated by the relatively low release of available energy into the C_5H_3 translational degrees of freedom along with its distribution at all angles in the center-of-mass frame.

The paths connecting $C_2(X^1\Sigma_g^+/a^3\Pi_u)$ plus $CH_3CCH(X^1A_1)$ to the 2,4-pentadiynyl-1 ($H_2CCCCCH$) and 1,4-pentadiynyl-3 (HCCCHCCH) radicals via atomic hydrogen loss on the C_5H_4 potential energy surface involve multiple C_5H_4 intermediates. On the singlet surface $H_2CCCCCH$ (**p2$_{MA}$**) is formed alongside the slightly less stable HCCCHCCH isomer (**p1$_{MA}$**) with respective yields of 65% and 32% at 20 kJ mol^{-1} as determined by RRKM.[99] C_5H_3 formation on the singlet surface requires as few as two intermediates by $C_2(X^1\Sigma_g^+)$ addition across the acetylene group, while on the triplet surface a minimum of four intermediates is required if addition similarly occurs across the CH_3CCH triple bond and only two intermediates

if $C_2(a^3\Pi_u)$ adds to the terminal (≡**C**−H) carbon atom.[101] On the triplet surface production of the $H_2CCCCCH$ isomer (**p2$_{MA}$**) is strongly preferred to HCCCHCCH (**p1$_{MA}$**) due to the rate determining [**t4**] → [**t5**] and [**t3**] → [**t8**] transition states, with the former being about 6 times faster than the latter.[101] The methyl-bearing *cis*-2,3,4-pentatrien-2,5-diyl [**t7**] intermediate, accessed via the relatively loose [**t4**] → [**t5**] ring-opening transition state, is thus favored for dissociation to 2,4-pentadiynyl-1 + H. Note that while hydrogen atom loss from the central carbon of [**t8**] is also possible, we did not observe a hydrogen loss channel using the d3-methylacetylene (CD_3CCH) isotopologue and thus exclude the formation $H_2CCCCCH$ via this path. Therefore, those dissociation products formed via [**t8**] do not contribute to our reactive scattering signal. Furthermore, the absence of an atomic hydrogen loss also removes the CH_3CCCC (**p4$_{MA}$**) isomer from consideration and thus C_5H_3 formation on the triplet surface is limited to $H_2CCCCCH$ (**p2$_{MA}$**). Considering the CM translational flux distribution $P(E_T)$, the plateau spanning $3 \leq E_T \leq 23$ kJ mol^{-1} (Figure 10) suggests at least two reaction pathways are responsible for C_5H_3 formation, where the distribution maximum contains information about the unimolecular dissociation of $[C_5H_4]^*$. As discussed, $H_2CCCCCH$ (**p2$_{MA}$**) is formed on the triplet surface via the [**t7**] intermediate only. On the singlet surface, both $H_2CCCCCH$ (**p2$_{MA}$**) and HCCCHCCH (**p1$_{MA}$**) are predicted to form with a relative yield of 2:1. The absence of a strong sideways peaking of the CM angular flux distribution might hint to a lack of significant reactive scattering signal arising from the singlet surface – i.e. a triplet rich dicarbon beam – where geometrical constraints on the decomposition of the highly symmetric methyldiacetylene [**s3**] intermediate would otherwise manifest in $T(\theta)$ by a maximum near $\theta = 90°$ for the C_5H_3 product.

Notably, the energetics forming C_5H_3 product isomers plus atomic hydrogen of −181 ± 25 kJ mol^{-1} are identical within the error limits to those derived by Guo et al. of −182 ± 10 kJ mol^{-1},[66] who sourced their dicarbon beam from graphite ablation. In the experiment conducted by Guo et al., the resulting data were best fit with a backward peaking $T(\theta)$ that featured a maximum near $\theta = 100°$.[66] The sideways character of this distribution was attributed to a decomposing methyldiacetylene intermediate where the departing hydrogen atom held a perpendicular trajectory with respect to the rotational plane of the $[C_5H_4]^*$ to form $H_2CCCCCH$ (**p2$_{MA}$**) and was later corroborated by the singlet potential energy surface of Mebel et al. that indicates a C_{3v} symmetric methyldiacetylene intermediate that precedes dissociation via

hydrogen atom emission from the methyl group.[99] In contrast with the ablation-sourced dicarbon experiment performed by Guo et al.,[66] our center-of-mass angular distribution is slightly forward and does not depict a maximum near $\theta = 90°$ (Figure 10). The change in *T(θ)* polarization, i.e. forward vs backward scattering of C_5H_3 products, is likely due to the difference in collision energies E_C employed in the two sets of experiments with $E_C = 37.6 \pm 0.8$ kJ mol^{-1} in the ablation study (compare to the much lower $E_C = 23.2 \pm 0.3$ kJ mol^{-1} used in the present study). Furthermore, the distribution maximum at *T(100°)* by Guo et al. attributed to the formation of 2,4-pentadiynyl-1 on the singlet surface via [**s3**] → **p2$_{MA}$** + H (Figure 15) is noticeably absent from the *T(θ)* derived in the present study (Figure 10). The dissimilarity of CM angular flux distributions in polarization and behavior near $\theta = 90°$ highlight a change in the reaction mechanism most representative of C_5H_3 + H formation in the two studies which could owe to differing $C_2(a^3\Pi_u)/C_2(X^1\Sigma_g^+)$ ratios derived from the ablation and photolytic dicarbon sources.

In the dicarbon plus methylacetylene (CH_3CCH) reaction we also probed for methyl-loss products at *m/z* 49 (C_4H^+) but detected no signal indicative of product formation. On the singlet surface (Figure 15), the $C_4H + CH_3$ product channel is exoergic by 20 kJ mol^{-1} but statistically accounts for about 5 of every million dissociation products at $E_C = 20$ kJ mol^{-1}. Through extension of the triplet surface formulated by Gu et al.[101] we identified three distinct $C_4H + CH_3$ dissociation channels on the triplet surface: two endoergic pathways leading to cyclic moieties and an exoergic route that produces the butadiynyl radical plus atomic hydrogen through the liberation of 70 kJ mol^{-1} (Figure 16, red paths); the noticeable difference in the energy of the $C_4H + CH_3$ product in the present calculations is attributed to the use of the higher CCSD(T)-F12/cc-pVTZ-f12 level of theory as compared to the G2M(RCC,MP2) level employed in the previous work.[99] The combined branching ratio for these channels is negligibly low and thus the absence of a product signal corresponding to $C_4H + CH_3$ in our $C_2(X^1\Sigma_g^+/a^3\Pi_u) + CH_3CCH$ reaction system is consistent with the existing theoretical framework.

Finally, in our dicarbon plus d3-methylacetylene (CD_3CCH) system we observed only the atomic deuterium channel leading to C_5HD_2 + D from which we derived a reaction energy of -169 ± 25 kJ mol^{-1}. This closely agrees with the formation of the $D_2CCCCCH$ and/or DCCCHCCD isomer(s) from the $C_2(X^1\Sigma_g^+/a^3\Pi_u) + CH_3CCH$ potential energy surface (Figures

15 and 16). On the singlet surface, both the $D_2CCCCCH$ and DCCCHCCD products can be formed by deuterium atom emission from intermediate [**s3**], [**s4**], or [**s5**] (Figure 15). On the triplet surface, the path through [**t8**], here considered as $D_2CCCHCCD$, can undergo atomic hydrogen emission from the central carbon to form $D_2CCCCCD$ + H, or atomic deuterium loss from the [**t8**] methylene group to form DCCCHCCD + D; however, the absence of the hydrogen loss channel suggests that the unimolecular dissociation of [**t8**] does not contribute to product formation as measured by the signal recorded at *m/*z 65 ($C_5HD_2^+$). Product formation on the triplet surface thus lies with the statistically favored path to dissociation via intermediate [**t7**], here $D_3CCCCCH$, by deuterium atom emission from the d3-methyl (CD_3) group to form $D_2CCCCCH$ + D. Note that absence of a hydrogen loss channel in the dicarbon plus d3-methylacetylene reaction system parallels the experimental outcome of Gu et al.[101]

4.2. Dicarbon – 1-Butyne

In our reactive scattering of dicarbon with 1-butyne we found that the reaction favors C_5H_3 emission in an overall exoergic reaction (−92 ± 16 kJ mol^{-1}). To assign a structure to the product formed in our experiment we turned to the $C_2(X^1\Sigma_g^+/a^3\Pi_u)$ plus $C_2H_5CCH(X_1A')$ potential energy surfaces formulated by Parker et al. (Figure 5 in reference 68) which contained a single methyl-loss forming the $H_2CCCCCH$ (**p2$_{1b}$**) propargyl analog. We extended the existing *triplet* C_6H_6 potential energy surface at the CCSD(T)/CBS(dt) level of theory to include pathways leading to three additional methyl-loss product channels: **p11$_{1b}$** + CH_3 (−91 kJ mol^{-1}), **p12$_{1b}$** + CH_3 (−29 kJ mol^{-1}), and **p13$_{1b}$** + CH_3 (−25 kJ mol^{-1}). The C_5H_3 products **p2$_{1b}$**, **p11$_{1b}$**, **p12$_{1b}$**, & **p13$_{1b}$** were further explored at CCSD(T) using the CBS(dtq) basis set resulting in reaction energies of −281, −86, −30, & −21 kJ mol^{-1} for each respective methyl-loss channel. The energies derived from the CCSD(T)/CBS(dt) and CCSD(T)/CBS(dtq) methods are accurate to within ± 15 kJ mol^{-1} and ± 10 kJ mol^{-1}, respectively. Importantly, viable pathways forming **p11$_{1b}$**, **p12$_{1b}$**, or **p13$_{1b}$** do not exist on the singlet surface. The relevant intermediates and transition states connecting $C_2(a^3\Pi_u)$ + $C_2H_5CCH(X^1A')$ to the aforementioned C_5H_3 + CH_3 product channels are compiled in Figure 18 and discussed below.

On the C_2 + C_2H_5CCH singlet surface (Figure 17), dicarbon adds to the triple bond (−**C**≡**C**−) of 1-butyne forming either a three-membered [**i1$_{1b}$**] or four-membered [**i2$_{1b}$**] ring intermediate. Intermediate [**i1$_{1b}$**] is connected to [**i2$_{1b}$**], and both ultimately to [**i3$_{1b}$**] which lies 602 kJ mol^{-1} below $C_2(X^1\Sigma_g^+)$ + $C_2H_5CCH(X^1A')$. From [**i3$_{1b}$**], three dissociation channels are accessible but only one involves methyl-loss: **p2$_{1b}$** + CH_3. The surface involving triplet C_2 is decisively more complex with an increased number of initial addition complexes that are both cyclic and acyclic (Figure 18). Specifically, the triplet reaction can proceed by barrierless addition of $C_2(a^3\Pi_u)$ to one or both carbon atoms in the C_2H_5−**C**≡**C**−H acetylene group. Addition to the terminal (≡**C**−H) or ethyl-substituted (≡**C**−C_2H_5) carbon yields the dicarbon-substituted intermediates [**i8$_{1b}$**] and [**i5$_{1b}$**], respectively. Dicarbon can also add barrierlessly to both acetylenic carbon atoms simultaneously (−**C**≡**C**−) forming a disubstituted tricarbon ring [**i4$_{1b}$**] that can isomerize to [**i5$_{1b}$**] or directly to [**i8$_{1b}$**] by ring opening via 60 kJ mol^{-1} and 62 kJ mol^{-1} barriers, respectively. Intermediate [**i5$_{1b}$**] is also connected to [**i8$_{1b}$**] by intermediate [**i6$_{1b}$**] which bears a tetracarbon ring and is the least stable C_6H_6 isomer on our triplet PES at 138 kJ mol^{-1} below the separated reactants. The four-membered ring of [**i6$_{1b}$**] can open to give the five-carbon chain structures [**i7$_{1b}$**] or [**i8$_{1b}$**] through respective barriers of 94 or 52 kJ mol^{-1}. From [**i7$_{1b}$**] and [**i8$_{1b}$**], several paths leading to numerous C_6H_6 intermediates and C_6H_5 product channels along with the resonantly stabilized *c*-C_5H_5 radical were developed, but are beyond this scope of this discussion. An extensive summary of these pathways is given by Parker et al. (2014).[68]

The products **p2$_{1b}$**, **p11$_{1b}$**, **p12$_{1b}$**, & **p13$_{1b}$** are attainable through C−CH_3 bond cleaving transition states from the methylated intermediates [**i4$_{1b}$**], [**i6$_{1b}$**], [**i7$_{1b}$**], and [**i8$_{1b}$**]. Intermediate [**i4$_{1b}$**], which is stabilized by 191 kJ mol^{-1} relative to the separated reactants, can form **p13$_{1b}$** + CH_3 through an exit barrier that lies 33 kJ mol^{-1} above the bimolecular entrance channel. [**i6$_{1b}$**] is bound by 138 kJ mol^{-1} and can yield **p12$_{1b}$** + CH_3 by barrierless dissociation. Intermediate [**i7$_{1b}$**] is stabilized by 197 kJ mol^{-1} and leads to the energetically most favorable methyl-loss channel, **p2$_{1b}$** + CH_3, via a barrier located 35 kJ mol^{-1} above the separated products. Intermediate [**i8$_{1b}$**] lies 210 kJ mol^{-1} below the separated reactants and can form **p11$_{1b}$** + CH_3 via a transition state 34 kJ mol^{-1} above this product channel.

Considering the collision energy of our C_2 + C_2H_5CCH reaction system, along with the rovibrational excitation in dicarbon's $X^1\Sigma_g^+$ and $a^3\Pi_u$ states, all C_5H_3 + CH_3 product channels are open under our experimental conditions. A comparison of the experimentally derived reaction energy (-92 ± 16 kJ mol^{-1}) with the C_5H_3 isomers **p2$_{1b}$**, **p11$_{1b}$**, **p12$_{1b}$**, & **p13$_{1b}$** formed in tandem with the methyl radical indicates that **p11$_{1b}$** + CH_3 (-86 ± 10 kJ mol^{-1}) most readily agrees with the experiment. The **p11$_{1b}$** ($H_2CCCHCC$) product is only formed on the triplet surface via $C_2(a^3\Pi_u)$ + $C_2H_5CCH(X^1A')$, and only by methyl emission from [**i8$_{1b}$**]. Hence the following mechanisms are feasible: **C_2 + C_4H_6** → [**i4$_{1b}$** → **i5$_{1b}$** → **i6$_{1b}$** → **i8$_{1b}$**] / [**i4$_{1b}$** → **i8$_{1b}$**] / [**i5$_{1b}$** → **i6$_{1b}$** → **i8$_{1b}$**] / [**i8$_{1b}$**] → **p11$_{1b}$** + **CH_3**. RRKM analysis indicates that the path through [**i4$_{1b}$**] → [**i8$_{1b}$**] is favored in the formation of **p11$_{1b}$** + CH_3. Our CM flux distributions cannot completely exclude the formation of the less stable C_5H_3 isomers **p12$_{1b}$** and **p13$_{1b}$**, whose minor contributions would be obscured by the imposing **p11$_{1b}$** + CH_3 channel. On the other hand, evidence for the rather exoergic **p2$_{1b}$** ($H_2CCCCCH$) + CH_3 channel is absent from the experimental data; this is consistent with the inherent higher barriers involved in the [**i5$_{1b}$**] → [**i6$_{1b}$**] → [**i7$_{1b}$**] reaction sequence. While we can positively attribute **p11$_{1b}$** formation to the $C_2(a^3\Pi_u)$ + $C_2H_5CCH(X^1A')$ reaction, we have not accounted for the most exoergic methyl-loss channel. On the triplet surface, RRKM calculations predict that $H_2CCCHCC$ (**p11$_{1b}$**) is produced alongside $H_2CCCCCH$ (**p2$_{1b}$**) with a relative yield of 7:1. On the singlet surface, however, $H_2CCCCCH$ (**p2$_{1b}$**) is expected to be the dominant product representing 92% of the total yield via intermediates [**i2**] and [**i3**].[68] The $a^3\Pi_u$ / $X^1\Sigma_g^+$ ratio in our dicarbon beam could be much greater than unity. Spectroscopic signatures for the singlet ground state with vibrational excitation up to v=1 were recorded, but we are unable to quantify the concentration of singlet species in the beam. One indicator may be in the CM functions for the C_2 + CH_3CCH reactions conducted in this study, specifically the polarization of the *T(θ)* flux distribution where characteristics of a singlet reaction coordinate are absent. Therefore, the highly favored $H_2CCCCCH$ (**p2$_{1b}$**) formation on the singlet surface may be negated by a reduced fraction of singlet dicarbon in the beam.

5. Conclusion

The crossed molecular beam technique was exploited to explore the formation of three isomers of resonantly stabilized (C_5H_3) radicals along with their d_2-substituted counterparts via the

bimolecular reactions of singlet/triplet dicarbon [$C_2(X^1\Sigma_g^+/a^3\Pi_u)$] with methylacetylene [$CH_3CCH(X^1A_1)$], d_3-methylacetylene [$CD_3CCH(X^1A_1)$], and 1-butyne [$C_2H_5CCH(X^1A')$] at collision energies of 23.2 ± 0.3, 24.0 ± 0.2, and 26.2 ± 0.8 kJ mol^{-1}, respectively, through chemically activated singlet/triplet C_5H_4/C_5D_3H and C_6H_6 intermediates. Considering the experimental challenges of graphite ablation sources as a dicarbon precursor, our present study utilize a newly developed supersonic dicarbon [$C_2(X^1\Sigma_g^+/a^3\Pi_u)$] beam generated via photolysis of helium-seeded tetrachloroethylene [$C_2Cl_4(X^1A_g)$]. The number densities of dicarbon of this photolysis source are higher by a factor of 2.5 compared to ablation sources with significantly enhanced speed ratios of up to about 12. Most importantly, the photolytic source eliminates the generation of carbon atoms, which are dominating co-reactants in ablation-based dicarbon sources thus hindering the detection of potential methyl loss channels. We first demonstrated the performance of our dicarbon [$C_2(X^1\Sigma_g^+/a^3\Pi_u)$] beam in reactions with methylacetylene [$CH_3CCH(X^1A_1)$] and d_3-methylacetylene [$CD_3CCH(X^1A_1)$] and demonstrated that the reaction dynamics match previous studies of these systems in our laboratory utilizing ablation-based dicarbon sources. These involve the formation of 1,4-pentadiynyl-3 [$HCCCHCCH(X^2B_1)$] and 2,4-pentadiynyl-1 [$H_2CCCCCH(X^2B_1)$] via atomic hydrogen (deuterium) atom elimination via overall barrierless and exoergic reactions on the singlet and triplet surfaces; no methyl-loss channel was detected, which correlated with predictions from RRKM calculations.

We also examined the $C_2(X^1\Sigma_g^+/a^3\Pi_u)$ - 1-butyne [$C_2H_5CCH(X^1A')$] reaction for the hitherto elusive methyl-loss pathway and detected reactive scattering signal at *m/z* 63 ($C_5H_3^+$) with a laboratory angular distribution characteristic of indirect scattering dynamics. The experimentally derived reaction energy of −92 ± 16 kJ mol^{-1} matches the computationally predicted product channel forming the resonantly stabilized penta-1-yn-3,4-dienyl-1 ($H_2CCCHCC$; X^2A) radical along with the methyl radical $CH_3(X^2A_2'')$. This channel is exclusively open on the triplet surface with an overall reaction energy of −86 ± 10 kJ mol^{-1}. The preferred reaction pathways proceed via barrier-less addition of triplet dicarbon to the π-electronic system of 1-butyne to both or to the sterically more accessible carbon atom via methyl-bearing triplet C_6H_6 intermediates [**i4$_{1b}$**] and [**i8$_{1b}$**], respectively, with the latter decomposing via a tight exit transition state to penta-1-yn-3,4-dienyl-1 ($H_2CCCHCC$; X^2A) plus the methyl radical $CH_3(X^2A_2'')$. It should be recalled that based on its reactivity and open shell character, triplet dicarbon has been dubbed a 'pseudo-halogen'. The addition of triplet dicarbon to the α-carbon atom of 1-butyne leading to [**i8$_{1b}$**]

followed by methyl group loss mirrors the addition – hydrogen/methyl group loss sequence in alkyne – halogen systems and also resembles the dicarbon addition – hydrogen atom sequence in the reaction of dicarbon with benzene forming the phenylethynyl radical (C_6H_5CC; X^2A').[74] The successful unraveling of this methyl-loss channel demonstrates the viability of the photolytically generated dicarbon beam as an unprecedented tool to probe the underlying reaction dynamics involved in the formation of resonantly stabilized free radicals (RSFR) – and in particular of exotic radicals formed via one-step triplet dicarbon addition – hydrogen/methyl loss elimination sequences highlighting the role of dicarbon as a pseudo halogen - of vital importance in molecular mass growth processed leading ultimately to polycyclic aromatic hydrocarbons (PAHs) previously beyond the reach of the crossed molecular beams community.

Conflicts of interest

There are no conflicts to declare.

Acknowledgements

This work was supported by the US Department of Energy, Basic Energy Sciences DE-FG02-03ER15411 and DE-FG02-04ER15570 to the University of Hawaii and to Florida International University, respectively.

References

1. R. Bleekrode and W. C. Nieuwpoort, *J. Chem. Phys.*, 1965, **43**, 3680-3687.
2. G. M. Lloyd and P. Ewart, *J. Chem. Phys.*, 1999, **110**, 385-392.
3. M. Hausmann and K. H. Homann, *Ber. Bunsenges. Phys. Chem.*, 1997, **101**, 651-667.
4. D. L. Lambert, Y. Sheffer, A. C. Danks, C. Arpigny and P. Magain, *Astrophys. J.*, 1990, **353**, 640-653.
5. M. R. Combi and U. Fink, *Astrophys. J.*, 1997, **484**, 879-890.
6. R. Gredel, *Astron. Astrophys.*, 1999, **351**, 657-668.
7. D. L. Lambert, Y. Sheffer and S. Federman, *Astrophys. J.*, 1995, **438**, 740-749.
8. G. da Silva and A. J. Trevitt, *Phys. Chem. Chem. Phys.*, 2011, **13**, 8940-8952.
9. M. Asplund, N. Grevesse, A. J. Sauval, C. Allende Prieto and R. Blomme, *Astron. Astrophys.*, 2005, **431**, 693-705.
10. M. Asplund, N. Grevesse, A. J. Sauval and P. Scott, *Annu. Rev. Astron. Astrophys.*, 2009, **47**, 481-522.
11. A. Drazdauskas, G. Tautvaišienė, S. Randich, A. Bragaglia, Š. Mikolaitis and R. Janulis, *Astron. Astrophys.*, 2016, **589**, A50.
12. A. C. Danks and D. L. Lambert, *Astron. Astrophys.*, 1983, **124**, 188-196.
13. D. Crampton, A. P. Cowley and R. M. Humphreys, *Astrophys. J.*, 1975, **198**, L135-L137.
14. L. Začs, F. Musaev, B. Kaminsky, Y. Pavlenko, A. Grankina, J. Sperauskas and B. J. Hrivnak, *Astrophys. J.*, 2016, **816**, 1-14.
15. A. G. Gaydon and H. G. Wolfhard, *Symp. (Int.) Combust., [Proc.]*, 1953, **4**, 211-218.
16. G. P. Smith, C. Park, J. Schneiderman and J. Luque, *Combust. Flame*, 2005, **141**, 66-77.
17. M. Köhler, A. Brockhinke, M. Braun-Unkhoff and K. Kohse-Höinghaus, *J. Phys. Chem. A*, 2010, **114**, 4719-4734.
18. S. Shaik, D. Danovich, W. Wu, P. Su, H. S. Rzepa and P. C. Hiberty, *Nat. Chem.*, 2012, **4**, 195-200.
19. O. Krechkivska, G. B. Bacskay, T. P. Troy, K. Nauta, T. D. Kreuscher, S. H. Kable and T. W. Schmidt, *J. Phys. Chem. A*, 2015, **119**, 12102-12108.
20. O. Krechkivska, B. A. Welsh, J. N. Fréreux, K. Nauta, S. H. Kable and T. W. Schmidt, *J. Mol. Spectrosc.*, DOI: 10.1016/j.jms.2017.09.009.

21. A. M. Mebel and R. I. Kaiser, *Int. Rev. Phys. Chem.*, 2015, **34**, 461-514.
22. R. I. Kaiser, M. Yamada and Y. Osamura, *J. Phys. Chem. A*, 2002, **106**, 4825-4832.
23. X. Gu, R. I. Kaiser, A. M. Mebel, V. V. Kislov, S. J. Klippenstein, L. B. Harding, M. C. Liang and Y. L. Yung, *Astrophys. J.*, 2009, **701**, 1797-1803.
24. N. Balucani, F. Leonori, R. Petrucci, K. M. Hickson and P. Casavecchia, *Phys. Scr.*, 2008, **78**, 058117.
25. X. Gu, Y. Guo, A. M. Mebel and R. I. Kaiser, *J. Phys. Chem. A*, 2006, **110**, 11265-11278.
26. X. Gu, Y. Guo and R. I. Kaiser, *Int. J. Mass spectrom.*, 2005, **246**, 29-34.
27. R. I. Kaiser, N. Balucani, D. O. Charkin and A. M. Mebel, *Chem. Phys. Lett.*, 2003, **382**, 112-119.
28. F. Leonori, R. Petrucci, K. M. Hickson, E. Segoloni, N. Balucani, S. D. Le Picard, P. Foggi and P. Casavecchia, *Planet. Space Sci.*, 2008, **56**, 1658-1673.
29. F. Zhang, S. Kim, R. I. Kaiser and A. M. Mebel, *J. Phys. Chem. A*, 2009, **113**, 1210-1217.
30. Y.-L. Sun, W.-J. Huang, C.-H. Chin and S.-H. Lee, *J. Chem. Phys.*, 2014, **141**, 194305.
31. Y.-L. Sun, W.-J. Huang and S.-H. Lee, *J. Phys. Chem. Lett.*, 2015, **6**, 4117-4122.
32. S. T. Ridgway, D. N. B. Hall, S. G. Kleinmann, D. A. Weinberger and R. S. Wojslaw, *Nature*, 1976, **264**, 345-346.
33. S. P. Souza and B. L. Lutz, *Astrophys. J.*, 1977, **216**, L49-L51.
34. M. Guélin, S. Green and P. Thaddeus, *Astrophys. J.*, 1978, **224**, L27-L30.
35. H. Suzuki, M. Ohishi, N. Kaifu, S.-I. Ishikawa and T. Kasuga, *Publ. Astron. Soc. Jpn.*, 1986, **38**, 911-917.
36. M. Guélin, J. Cernicharo, C. Kahane, J. Gomez-Gonzalez and C. Walmsley, *Astron. Astrophys.*, 1987, **175**, L5-L8.
37. J. Lacy, N. J. Evans, J. Achtermann, D. Bruce, J. Arens and J. Carr, *Astrophys. J.*, 1989, **342**, L43-L46.
38. J. Cernicharo and M. Guélin, *Astron. Astrophys.*, 1996, **309**, L27-L30.
39. J. Cernicharo, A. M. Heras, A. G. G. M. Tielens, J. R. Pardo, F. Herpin, M. Guélin and L. B. F. M. Waters, *Astrophys. J., Lett.*, 2001, **546**, L123-L126.
40. R. I. Kaiser, W. Sun, A. G. Suits and Y. T. Lee, *J. Chem. Phys.*, 1997, **107**, 8713-8716.

41. R. I. Kaiser, A. M. Mebel and Y. T. Lee, *J. Chem. Phys.*, 2000, **114**, 231-239.
42. R. I. Kaiser, D. Stranges, Y. T. Lee and A. G. Suits, *Astrophys. J.*, 1997, **477**, 982.
43. R. I. Kaiser, A. M. Mebel, A. H. H. Chang, S. H. Lin and Y. T. Lee, *J. Chem. Phys.*, 1999, **110**, 10330-10344.
44. B. B. Dangi, S. Maity, R. I. Kaiser and A. M. Mebel, *J. Phys. Chem. A*, 2013, **117**, 11783-11793.
45. X. Gu, Y. Guo, F. Zhang, A. M. Mebel and R. I. Kaiser, *Chem. Phys.*, 2007, **335**, 95-108.
46. Y. Guo, X. Gu and R. I. Kaiser, *Int. J. Mass spectrom.*, 2006, **249**, 420-425.
47. S.-H. Lee, W.-J. Huang, Y.-C. Lin and C.-H. Chin, *Astrophys. J.*, 2012, **759**, 75.
48. R. I. Kaiser, M. Goswami, P. Maksyutenko, F. Zhang, Y. S. Kim, A. Landera and A. M. Mebel, *J. Phys. Chem. A*, 2011, **115**, 10251-10258.
49. R. I. Kaiser, P. Maksyutenko, C. Ennis, F. Zhang, X. Gu, S. P. Krishtal, A. M. Mebel, O. Kostko and M. Ahmed, *Faraday Discuss.*, 2010, **147**, 429-478.
50. P. Maksyutenko, F. Zhang, X. Gu and R. I. Kaiser, *Phys. Chem. Chem. Phys.*, 2011, **13**, 240-252.
51. F. Zhang, P. Maksyutenko and R. I. Kaiser, *Phys. Chem. Chem. Phys.*, 2012, **14**, 529-537.
52. R. I. Kaiser, C. C. Chiong, O. Asvany, Y. T. Lee, F. Stahl, P. von R. Schleyer and H. F. Schaefer, *J. Chem. Phys.*, 2001, **114**, 3488-3496.
53. F. Stahl, P. von Ragué Schleyer, H. F. Bettinger, R. I. Kaiser, Y. T. Lee and H. F. Schaefer, *J. Chem. Phys.*, 2001, **114**, 3476-3487.
54. B. M. Jones, F. Zhang, R. I. Kaiser, A. Jamal, A. M. Mebel, M. A. Cordiner and S. B. Charnley, *Proc. Natl. Acad. Sci. U. S. A.*, 2011, **108**, 452-457.
55. A. M. Mebel, V. V. Kislov and R. I. Kaiser, *J. Am. Chem. Soc.*, 2008, **130**, 13618-13629.
56. H. Jin, A. Frassoldati, Y. Wang, X. Zhang, M. Zeng, Y. Li, F. Qi, A. Cuoci and T. Faravelli, *Combust. Flame*, 2015, **162**, 1692-1711.
57. D. S. N. Parker, R. I. Kaiser, T. P. Troy, O. Kostko, M. Ahmed and A. M. Mebel, *J. Phys. Chem. A*, 2015, **119**, 7145-7154.
58. N. M. Marinov, W. J. Pitz, C. K. Westbrook, A. M. Vincitore, M. J. Castaldi, S. M. Senkan and C. F. Melius, *Combust. Flame*, 1998, **114**, 192-213.
59. A. M. Mebel and V. V. Kislov, *J. Phys. Chem. A*, 2009, **113**, 9825-9833.

60. Z. Tian, W. J. Pitz, R. Fournet, P.-A. Glaude and F. Battin-Leclerc, *Proc. Combust. Inst.*, 2011, **33**, 233-241.
61. B. Yang, Y. Li, L. Wei, C. Huang, J. Wang, Z. Tian, R. Yang, L. Sheng, Y. Zhang and F. Qi, *Proc. Combust. Inst.*, 2007, **31**, 555-563.
62. B. Yang, C. Huang, L. Wei, J. Wang, L. Sheng, Y. Zhang, F. Qi, W. Zheng and W.-K. Li, *Chem. Phys. Lett.*, 2006, **423**, 321-326.
63. N. Hansen, S. J. Klippenstein, J. A. Miller, J. Wang, T. A. Cool, M. E. Law, P. R. Westmoreland, T. Kasper and K. Kohse-Höinghaus, *J. Phys. Chem. A*, 2006, **110**, 4376-4388.
64. V. V. Kislov, T. L. Nguyen, A. M. Mebel, S. H. Lin and S. C. Smith, *J. Chem. Phys.*, 2004, **120**, 7008-7017.
65. A. M. Mebel, S. H. Lin, X. M. Yang and Y. T. Lee, *J. Phys. Chem. A*, 1997, **101**, 6781-6789.
66. Y. Guo, X. Gu, N. Balucani and R. I. Kaiser, *J. Phys. Chem. A*, 2006, **110**, 6245-6249.
67. Y. Guo, X. Gu, F. Zhang, A. M. Mebel and R. I. Kaiser, *J. Phys. Chem. A*, 2006, **110**, 10699-10707.
68. D. S. N. Parker, S. Maity, B. B. Dangi, R. I. Kaiser, A. Landera and A. M. Mebel, *Phys. Chem. Chem. Phys.*, 2014, **16**, 12150-12163.
69. N. Balucani, A. M. Mebel, Y. T. Lee and R. I. Kaiser, *J. Phys. Chem. A*, 2001, **105**, 9813-9818.
70. Y. Guo, V. V. Kislov, X. Gu, F. Zhang, A. M. Mebel and R. I. Kaiser, *Astrophys. J.*, 2006, **653**, 1577.
71. A. M. Mebel, R. I. Kaiser and Y. T. Lee, *J. Am. Chem. Soc.*, 2000, **122**, 1776-1788.
72. B. B. Dangi, D. S. N. Parker, R. I. Kaiser, D. Belisario-Lara and A. M. Mebel, *Chemical Physics Letters*, 2014, **607**, 92-99.
73. B. B. Dangi, D. S. N. Parker, T. Yang, R. I. Kaiser and A. M. Mebel, *Angew. Chem., Int. Ed.*, 2014, **53**, 4608-4613.
74. X. Gu, Y. Guo, F. Zhang, A. M. Mebel and R. I. Kaiser, *Chem. Phys. Lett.*, 2007, **436**, 7-14.
75. F. Zhang, B. Jones, P. Maksyutenko, R. I. Kaiser, C. Chin, V. V. Kislov and A. M. Mebel, *J. Am. Chem. Soc.*, 2010, **132**, 2672-2683.

76. X. Gu, Y. Guo, E. Kawamura and R. I. Kaiser, *Journal of Vacuum Science & Technology A: Vacuum, Surfaces, and Films*, 2006, **24**, 505-511.
77. N. Balucani, O. Asvany, A. H. H. Chang, S. H. Lin, Y. T. Lee, R. I. Kaiser, H. F. Bettinger, P. v. R. Schleyer and H. F. Schaefer, *J. Chem. Phys.*, 1999, **111**, 7472-7479.
78. L. C. L. Huang, Y. T. Lee and R. I. Kaiser, *J. Chem. Phys.*, 1999, **110**, 7119-7122.
79. L. C. L. Huang, N. Balucani, Y. T. Lee, R. I. Kaiser and Y. Osamura, *J. Chem. Phys.*, 1999, **111**, 2857-2860.
80. N. Balucani, O. Asvany, R. I. Kaiser and Y. Osamura, *J. Phys. Chem. A*, 2002, **106**, 4301-4311.
81. R. I. Kaiser, J. W. Ting, L. C. L. Huang, N. Balucani, O. Asvany, Y. T. Lee, H. Chan, D. Stranges and D. Gee, *Rev. Sci. Instrum.*, 1999, **70**, 4185-4191.
82. R. I. Kaiser, I. Hahndorf, L. C. L. Huang, Y. T. Lee, H. F. Bettinger, P. v. R. Schleyer, H. F. Schaefer and P. R. Schreiner, *The Journal of Chemical Physics*, 1999, **110**, 6091-6094.
83. I. Hahndorf, H. Y. Lee, A. M. Mebel, S. H. Lin, Y. T. Lee and R. I. Kaiser, *J. Chem. Phys.*, 2000, **113**, 9622-9636.
84. L. C. L. Huang, H. Y. Lee, A. M. Mebel, S. H. Lin, Y. T. Lee and R. I. Kaiser, *J. Chem. Phys.*, 2000, **113**, 9637-9648.
85. N. Balucani, H. Y. Lee, A. M. Mebel, Y. T. Lee and R. I. Kaiser, *J. Chem. Phys.*, 2001, **115**, 5107-5116.
86. Y. T. Lee, eds. G. Scoles, D. Bassi, U. Buck and D. Lainé, Oxford University Press New York, New York, NY, 1988, vol. 1, ch. Reactive Scattering I: Nonoptical Methods.
87. A. Fontijn, A. Fernandez, A. Ristanovic, M. Y. Randall and J. T. Jankowiak, *J. Phys. Chem. A*, 2001, **105**, 3182-3189.
88. A. Ristanovic, A. Fernandez and A. Fontijn, *J. Phys. Chem. A*, 2002, **106**, 8291-8295.
89. C. Huang, D. Zhao, L. Pei, C. Chen and Y. Chen, *Chem. Phys. Lett.*, 2004, **389**, 230--235.
90. C. Huang, Z. Zhu, H. Wang, L. Pei and Y. Chen, *J. Phys. Chem. A*, 2005, **109**, 3921-3925.
91. M. Nakajima, A. Matsugi and A. Miyoshi, *J. Phys. Chem. A*, 2009, **113**, 8963-8970.
92. A. Matsugi, K. Suma and A. Miyoshi, *J. Phys. Chem. A*, 2010, **114**, 4580-4585.

93. C. Huang, Z. Zhu, Y. Xin, L. Pei, C. Chen and Y. Chen, *J. Chem. Phys.*, 2004, **120**, 2225-2229.

94. A. Páramo, A. Canosa, S. D. Le Picard and I. R. Sims, *J. Phys. Chem. A*, 2008, **112**, 9591-9600.

95. R. I. Kaiser and A. G. Suits, *Rev. Sci. Instrum.*, 1995, **66**, 5405-5411.

96. I. C. Lu, W.-J. Huang, C. Chaudhuri, W.-K. Chen and S.-H. Lee, *Rev. Sci. Instrum.*, 2007, **78**, 083103.

97. M. Alagia, V. Aquilanti, D. Ascenzi, N. Balucani, D. Cappelletti, L. Cartechini, P. Casavecchia, F. Pirani, G. Sanchini and G. G. Volpi, *Isr. J. Chem.*, 1997, **37**, 329-342.

98. X. Gu, Y. Guo, F. Zhang, A. M. Mebel and R. I. Kaiser, *Faraday Discuss.*, 2006, **133**, 245-275.

99. A. M. Mebel, V. V. Kislov and R. I. Kaiser, *J. Phys. Chem. A*, 2006, **110**, 2421-2433.

100. A. M. Mebel, V. V. Kislov and R. I. Kaiser, in *Gas Phase Molecular Reaction and Photodissociation Dynamics*, eds. K. C. Lin and P. D. Kleiber, Transworld Research Network, Kerala, India, 2007, pp. 113-159.

101. X. Gu, Y. Guo, F. Zhang, A. M. Mebel and R. I. Kaiser, *Chem. Phys. Lett.*, 2007, **444**, 220-225.

102. G. O. Brink, *Rev. Sci. Instrum.*, 1966, **37**, 857-860.

103. N. R. Daly, *Rev. Sci. Instrum.*, 1960, **31**, 264-267.

104. D. Proch and T. Trickl, *Rev. Sci. Instrum.*, 1989, **60**, 713-716.

105. P. S. Weiss, PhD Ph.D. Dissertation, University of California, 1986.

106. M. F. Vernon, Ph.D. Ph.D. Dissertation, University of California, 1983.

107. F. Leonori, K. M. Hickson, S. D. Le Picard, X. Wang, R. Petrucci, P. Foggi, N. Balucani and P. Casavecchia, *Mol. Phys.*, 2010, **108**, 1097-1113.

108. W. Chen, K. Kawaguchi, P. F. Bernath and J. Tang, *J. Chem. Phys.*, 2015, **142**, 064317.

109. T. W. Schmidt and G. B. Bacskay, *J. Chem. Phys.*, 2007, **127**, 234310.

110. C. M. Western, *J. Quant. Spectrosc. Radiat. Transfer*, 2017, **186**, 221-242.

111. J. S. A. Brooke, P. F. Bernath, T. W. Schmidt and G. B. Bacskay, *J. Quant. Spectrosc. Radiat. Transfer*, 2013, **124**, 11-20.

112. T. Yang, B. B. Dangi, P. Maksyutenko, R. I. Kaiser, L. W. Bertels and M. Head-Gordon, *J. Phys. Chem. A*, 2015, **119**, 12562-12578.

113. A. D. Becke, *J. Chem. Phys.*, 1993, **98**, 5648-5652.
114. C. Lee, W. Yang and R. G. Parr, *Physical Review B*, 1988, **37**, 785-789.
115. G. D. Purvis and R. J. Bartlett, *The Journal of Chemical Physics*, 1982, **76**, 1910-1918.
116. T. H. Dunning, *The Journal of Chemical Physics*, 1989, **90**, 1007-1023.
117. S. B. Huh and J. S. Lee, *The Journal of Chemical Physics*, 2003, **118**, 3035-3042.
118. T. B. Adler, G. Knizia and H.-J. Werner, *The Journal of Chemical Physics*, 2007, **127**, 221106.
119. G. Knizia, T. B. Adler and H.-J. Werner, *The Journal of Chemical Physics*, 2009, **130**, 054104.
120. M. Frisch, G. Trucks, H. Schlegel, G. Scuseria, M. Robb, J. Cheeseman, G. Scalmani, V. Barone, B. Mennucci and G. Petersson, *GAUSSIAN 09, revision A.1*, Gaussian Inc., Wallingford, CT, 2009.
121. H.-J. Werner, P. Knowles, R. Lindh, F. R. Manby, M. Schütz, P. Celani, T. Korona, G. Rauhut, R. Amos and A. Bernhardsson, *MOLPRO, Version 2010.1, a package of ab initio programs*, University of Cardiff, Cardiff, UK, 2010, see http://www.molpro.net/.
122. P. J. Robinson and K. A. Holbrook, *Unimolecular Reactions*, John Wiley & Sons, Ltd., New York, NY, 1972.
123. H. Eyring, S. H. Lin and S. M. Lin, *Basic Chemical Kinetics*, John Wiley and Sons, Inc., New York, NY, 1980.
124. J. Steinfield, J. Francisco and W. Hase, *Chemical Kinetics and Dynamics*, Prentice Hall, Englewood Cliffs, NJ, 1982.
125. A. Largo, P. Redondo and C. Barrientos, *J. Am. Chem. Soc.*, 2004, **126**, 14611-14619.
126. D. S. N. Parker, B. B. Dangi, R. I. Kaiser, A. Jamal, M. Ryazantsev and K. Morokuma, *J. Phys. Chem. A*, 2014, **118**, 12111-12119.
127. R. D. Levine, *Molecular Reaction Dynamics*, Cambridge University Press, Cambridge, U.K., 2005.
128. A. V. Wilson, D. S. N. Parker, F. Zhang and R. I. Kaiser, *Phys. Chem. Chem. Phys.*, 2012, **14**, 477-481.

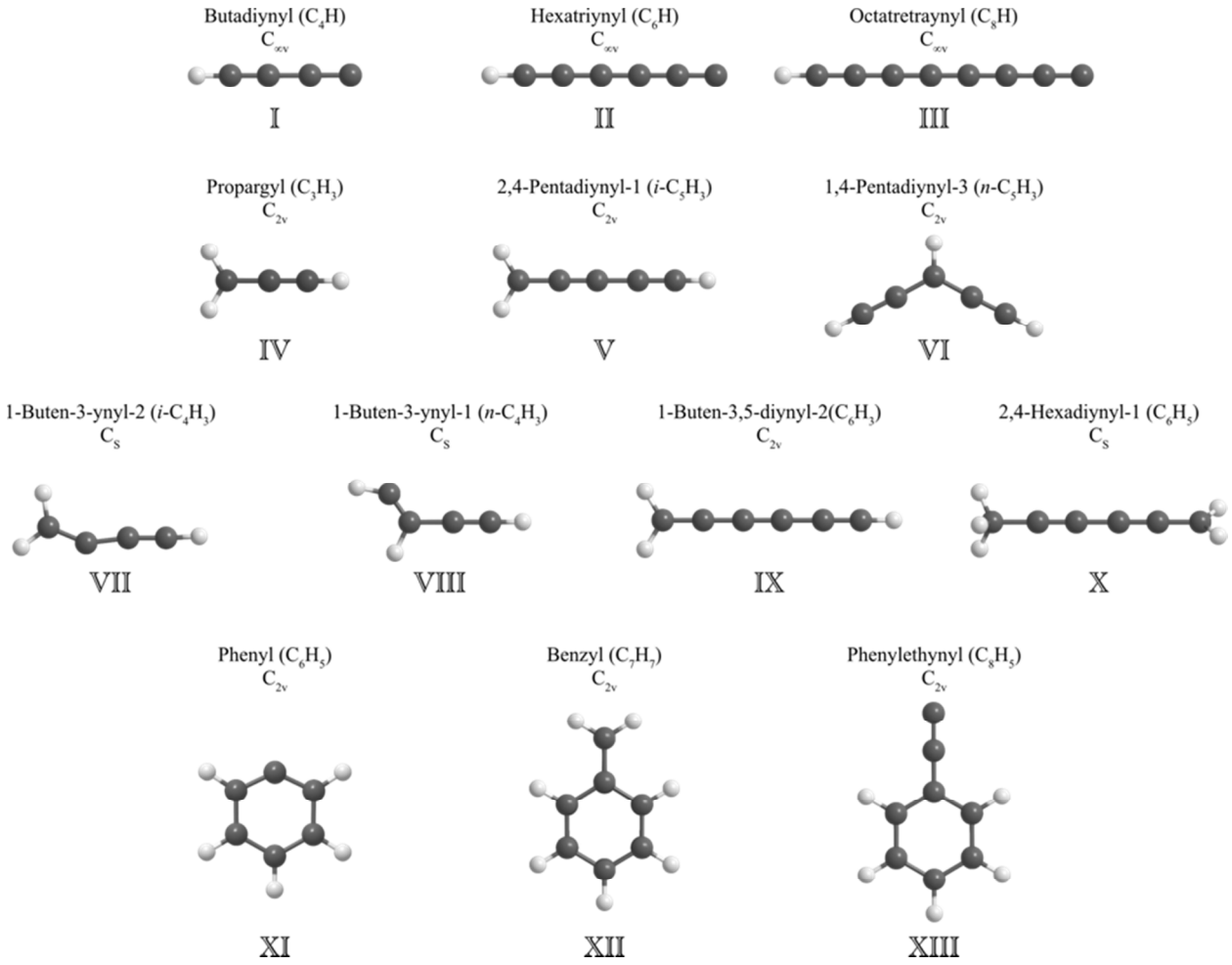

Scheme 1. Structures and point groups of selected radicals synthesized via bimolecular reactions of dicarbon with unsaturated hydrocarbons.

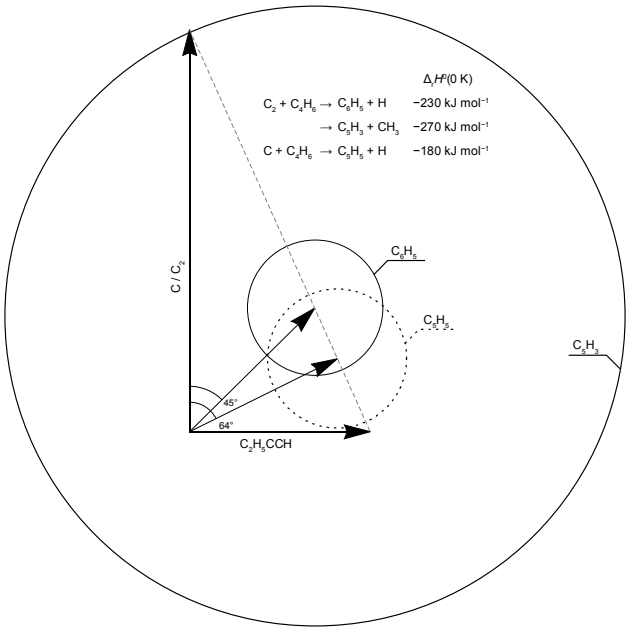

Figure 1. Newton diagram for the atomic hydrogen and methyl loss channels in the reaction of dicarbon ($C_2(X^1\Sigma_g^+)$) with 1-butyne (C_2H_5CCH) (solid circles); the atomic hydrogen loss channel for the atomic carbon – 1-butyne reaction is also shown (dashed circle).

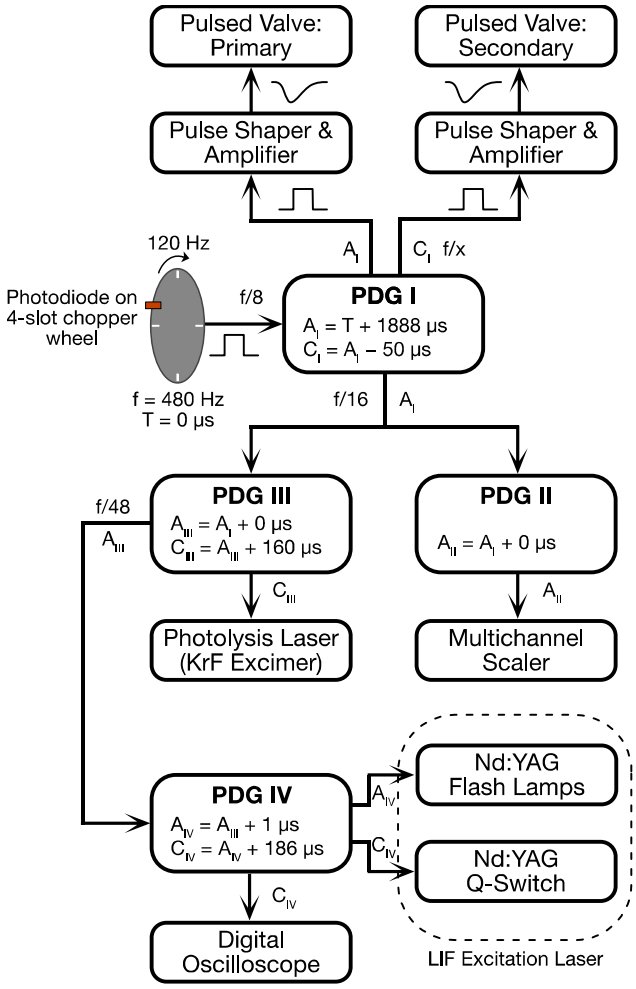

Figure 2. Pulse sequence applied or the crossed molecular beam reactions of dicarbon (C_2; $X^1\Sigma_g^+/\ a^3\Pi_u$) with methylacetylene (CH_3CCH; X^1A_1), d_3-methylacetylene (CD_3CCH; X^1A_1), and 1-butyne (C_2H_5CCH; X^1A'). The timing scheme used for the laser-induced fluorescence (LIF) for singlet and triplet dicarbon is also included. PDG: pulse/delay generator. x = 8 for methylacetylene and 1-butyne; x = 16 for d_3-methylacetylene.

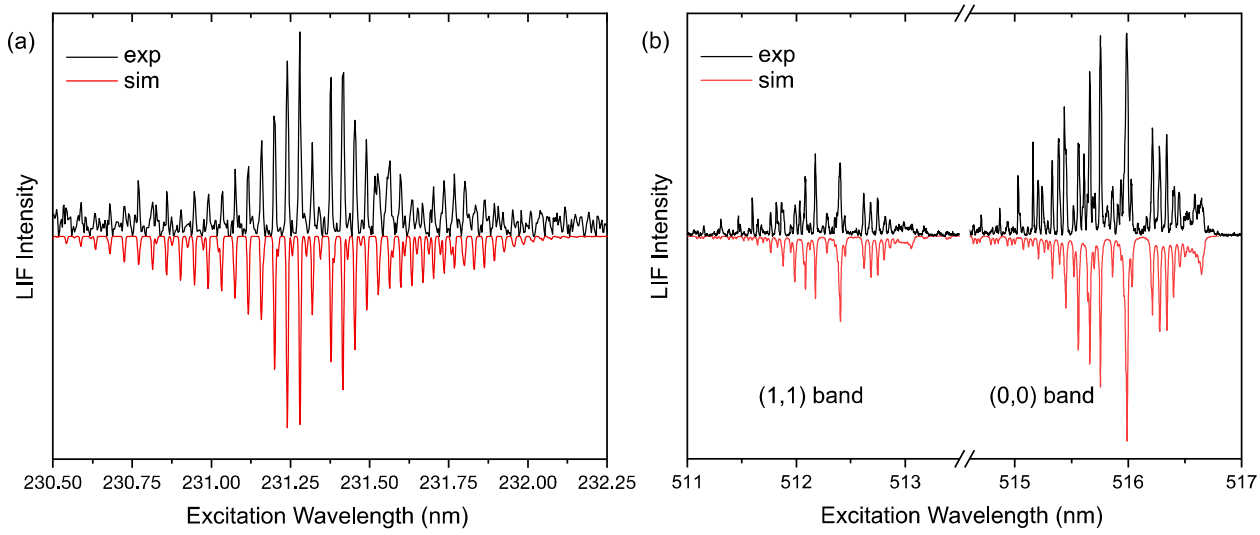

Figure 3. (a) Laser induced fluorescence (LIF) excitation spectrum of the Mulliken band ($D^1\Sigma_u^+ - X^1\Sigma_g^+$) in singlet dicarbon. (b) LIF excitation spectrum of the Swan band ($d^3\Pi_g - a^3\Pi_u$) in triplet dicarbon. Both the experimental spectrum (black) and best-fit simulation (red) are shown.

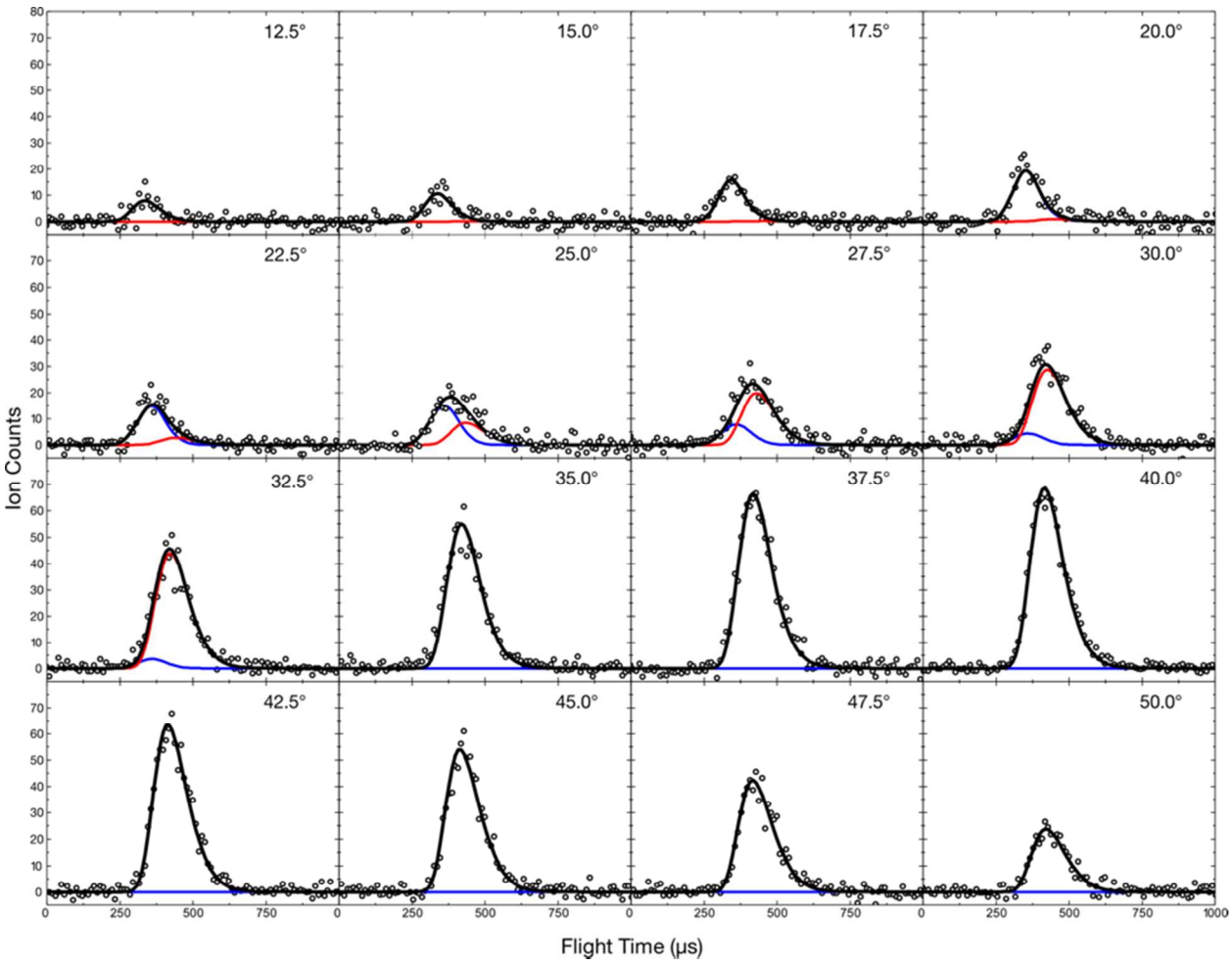

Figure 4. Time of flight (TOF) spectra (open circles) recorded at mass-to-charge ratio (*m/z*) 63 ($C_5H_3^+$) produced from the reaction of dicarbon (C_2) and chloroethynyl (C_2Cl) with methylacetylene (CH_3CCH) at various laboratory angles. Contributions to each TOF spectrum from dicarbon (C_2) and chloroethynyl (C_2Cl) channels are indicated by red and blue curves, respectively. The black line represents the sum of both channels.

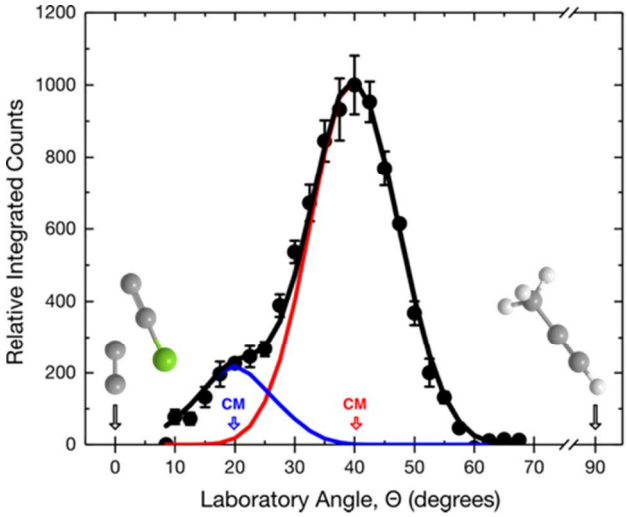

Figure 5. Laboratory angular distribution (LAD) recorded at mass-to-charge ratio (*m/z*) 63 ($C_5H_3^+$) produced from the reaction of dicarbon (C_2) and chloroethynyl (C_2Cl) with methylacetylene (CH_3CCH). Experimental data are indicated by black dots and the simulation represented by a black curve. Simulated contributions originating from dicarbon (C_2) and chloroethynyl (C_2Cl) channels are indicated by red and blue curves, respectively. CM defines the center of mass.

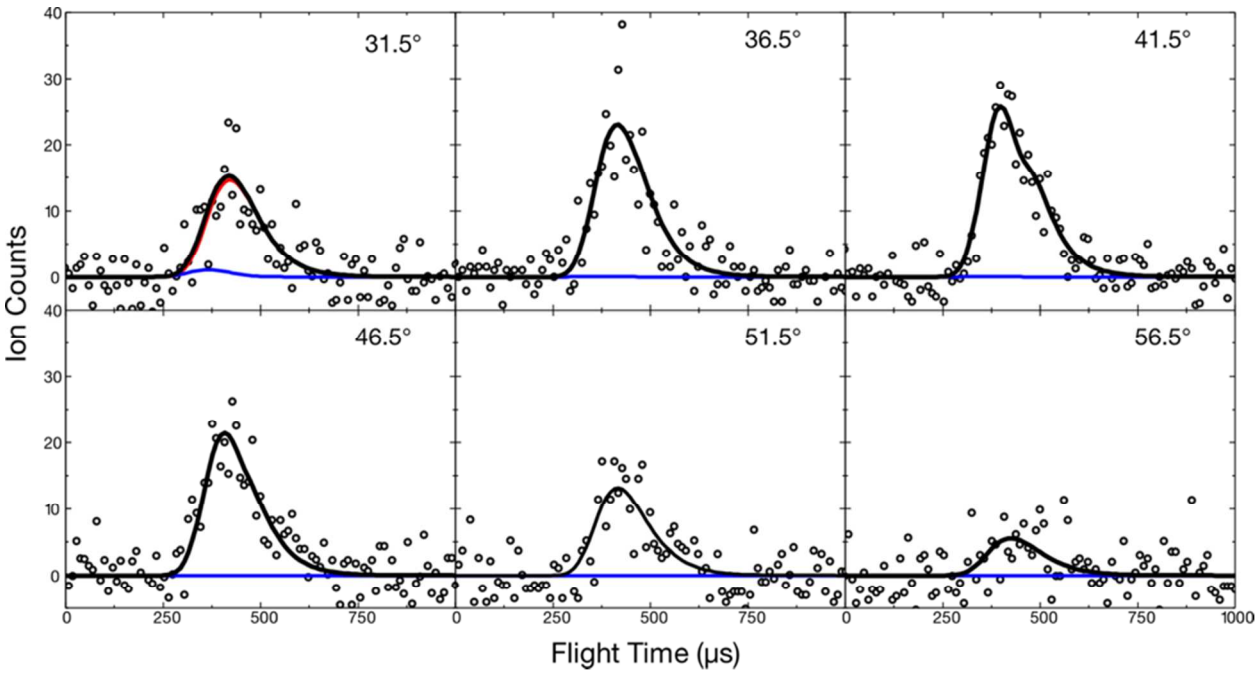

Figure 6. Time of flight (TOF) spectra (open circles) recorded at mass-to-charge ratio (*m/z*) 65 ($C_5HD_2^+$) produced from the reaction of dicarbon (C_2) and chloroethynyl (C_2Cl) with d_3-methylacetylene (CD_3CCH). Contributions to each TOF spectrum from dicarbon (C_2) and chloroethynyl (C_2Cl) channels are indicated by red and blue curves, respectively. The black line represents the sum of both channels.

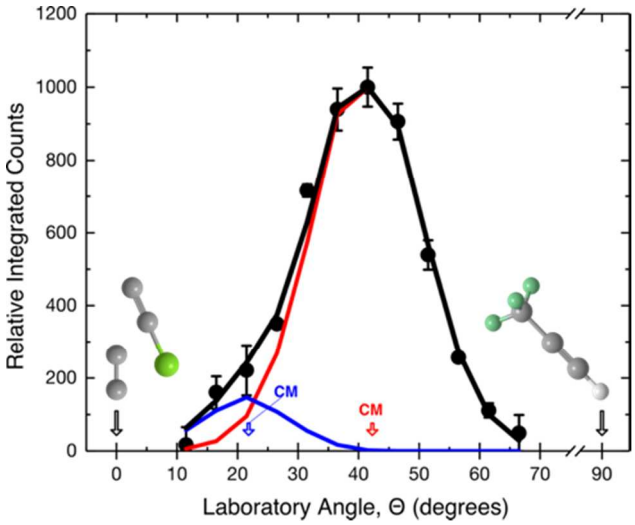

Figure 7. Laboratory angular distribution (LAD) recorded at mass-to-charge ratio (*m/z*) 65 ($C_5HD_2^+$) produced from the scattering of dicarbon (C_2) and chloroethynyl (C_2Cl) with d3-methylacetylene (CD_3CCH). Experimental data are indicated by black dots and the simulation represented by a black curve. Simulated contributions originating from dicarbon (C_2) and chloroethynyl (C_2Cl) channels are indicated by red and blue curves, respectively. CM defines the center of mass.

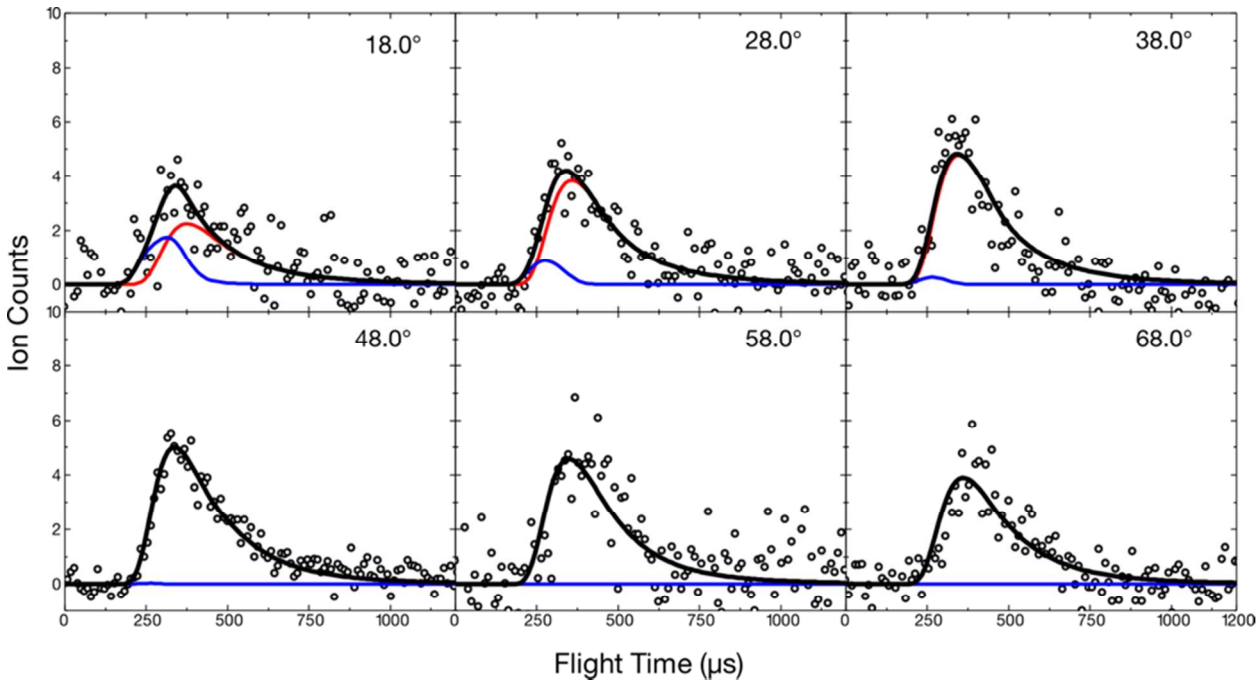

Figure 8. Time of flight (TOF) spectra (open circles) recorded at mass-to-charge ratio (*m/z*) 63 ($C_5H_3^+$) produced from the reactive scattering of dicarbon (C_2) with 1-butyne (C_2H_5CCH) at selected laboratory angles. Contributions to each TOF spectrum (black) from dicarbon (C_2) and non-reactive scattering are indicated by red and blue curves, respectively.

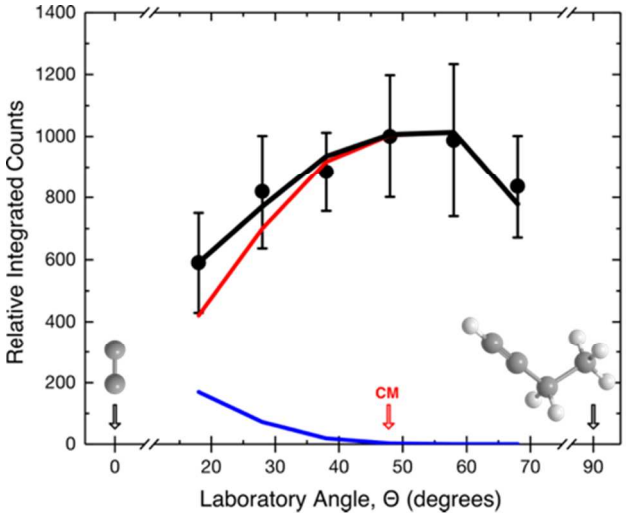

Figure 9. Laboratory angular distribution (LAD) recorded at mass-to-charge ratio (*m/z*) 63 ($C_5H_3^+$) produced from the scattering of dicarbon (C_2) with 1-butyne (C_2H_5CCH). Experimental data are indicated by black dots and the simulation represented by a black curve. The reactive and non-reactive scattering channels are indicated in red and blue, respectively. CM defines the center of mass.

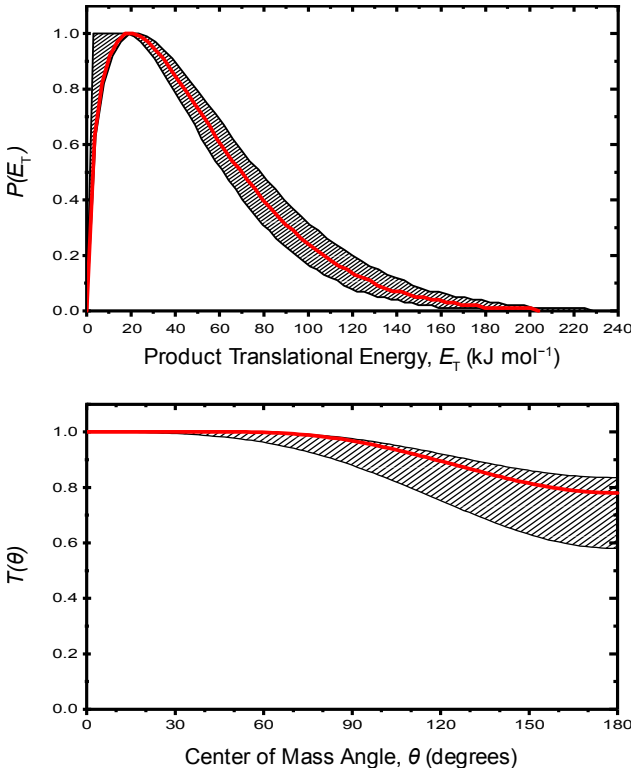

Figure 10. Center-of-mass translational energy $P(E_T)$ (upper) and angular $T(\theta)$ flux distributions (lower) of for the reaction of dicarbon with methylacetylene forming C_5H_3 isomers via an atomic hydrogen (H) emission. The best-fit functions are represented by red lines with error fitting indicated by hatching.

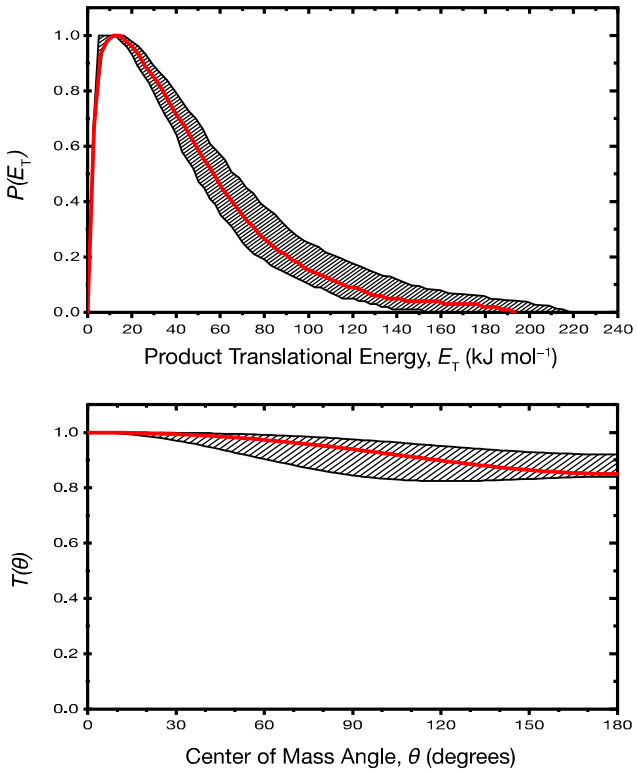

Figure 11. Center-of-mass translational energy $P(E_T)$ (upper) and angular $T(\theta)$ flux distributions (lower) of for the reaction of dicarbon with d_3-methylacetylene forming C_5HD_2 isomers via an atomic deuterium (D) emission. The best-fit functions are represented by red lines with error fitting indicated by hatching.

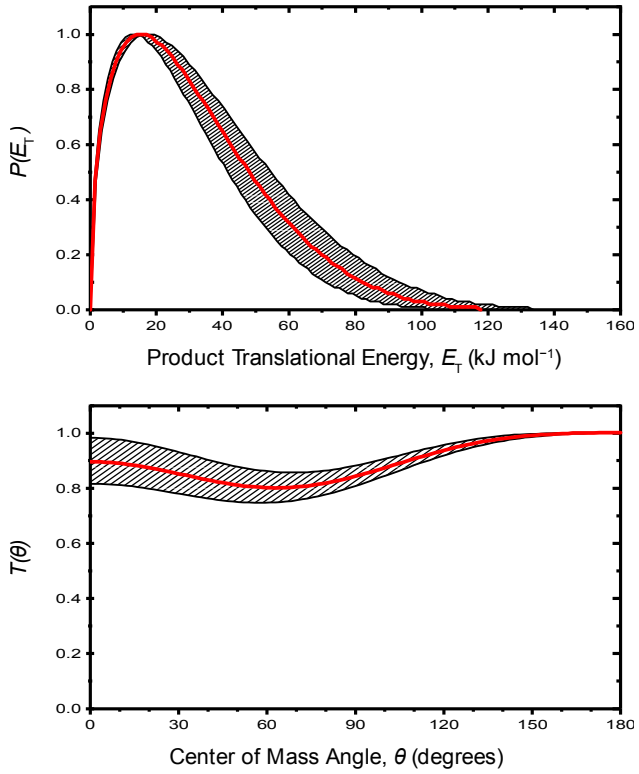

Figure 12. Center-of-mass translational energy $P(E_T)$ (upper) and angular $T(\theta)$ flux distributions (lower) of for the reaction of dicarbon with 1-butyne forming C_5H_3 isomers via methyl (CH_3) emission. The best-fit functions are represented by red lines with error fitting indicated by hatching.

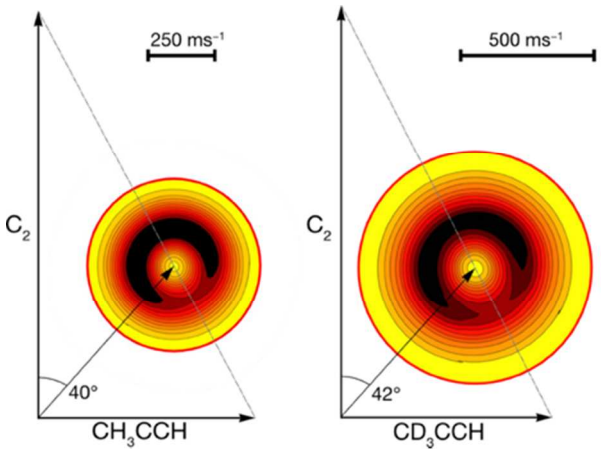

Figure 13. Newton diagrams of the distribution of C_5H_3 isomers formed via reactive scattering of dicarbon (C_2) with methylacetylene (CH_3CCH) (*left*) and d_3-methylacetylene (CD_3CCH) (*right*). The Newton circle (red) has a radius corresponding to the maximum velocity of C_5H_3 (or C_5HD_2) in the CM frame for each respective reaction and visualizes the flux distribution of heavy products as determined by the CM functions.

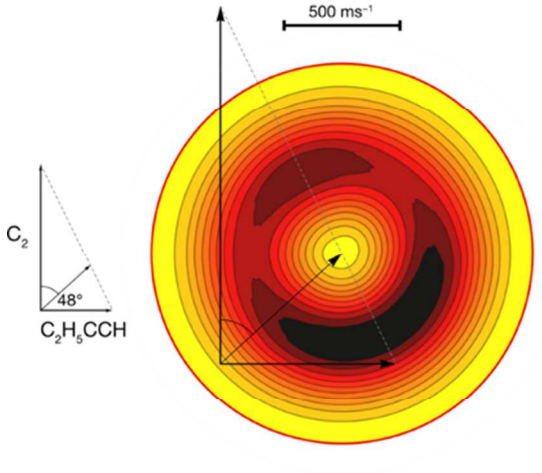

Figure 14. Newton diagram of the distribution of C_5H_3 isomers formed via reactive scattering of dicarbon (C_2) with 1-butyne (C_2H_5CCH). The Newton circle (red) has a radius corresponding to the maximum velocity of C_5H_3 in the CM frame and visualizes the flux distribution of C_5H_3 as determined by the CM functions.

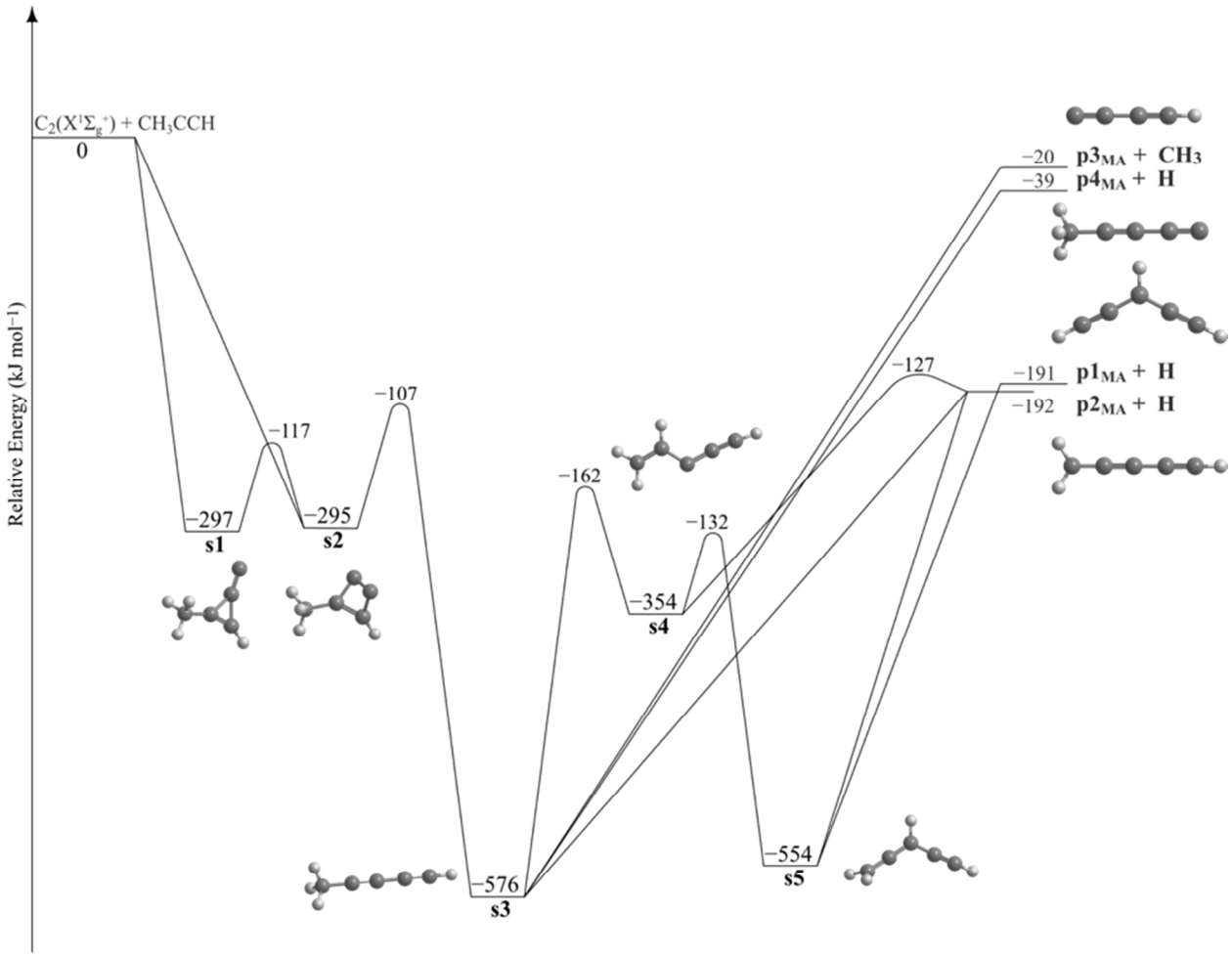

Figure 15. Schematic representation of the potential energy surface (PES) accessed by the reaction of dicarbon ($C_2(X^1\Sigma_g^+)$) plus methylacetylene (CH_3CCH (X^1A_1)) adopted from Mebel et al.[99] Energies are determined at the G2M(RCC,MP2) level of theory and given relative to the separated reactants in kJ mol^{-1}.

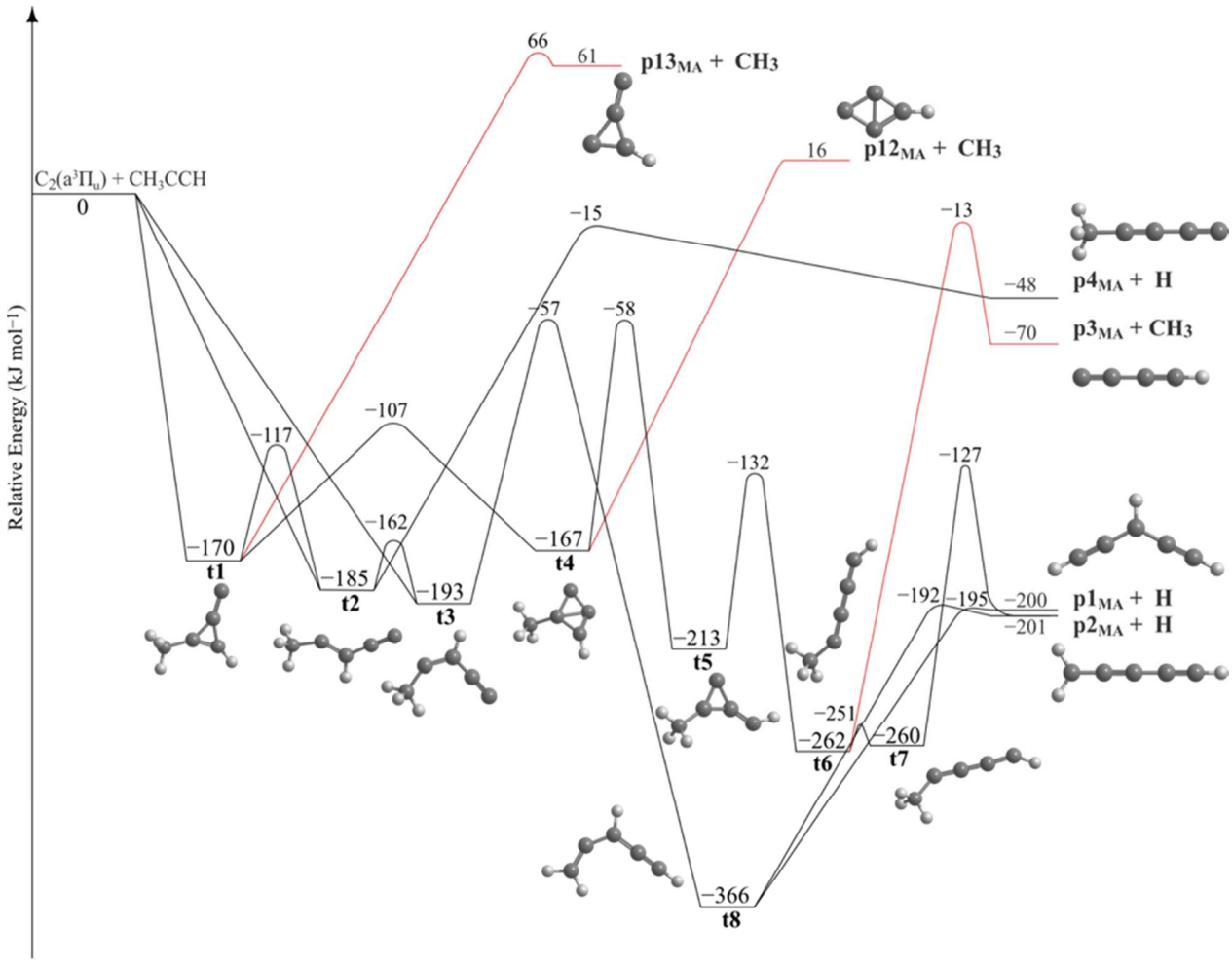

Figure 16. Schematic representation of the potential energy surface (PES) accessed by the reaction of dicarbon ($C_2(a^3\Pi_u)$) plus methylacetylene (CH_3CCH (X^1A_1)) adopted from Gu et al.[101] All energies are relative to the separated reactants and given in kJ mol^{-1}. New $C_4H + CH_3$ pathways developed in this study are shown in red.

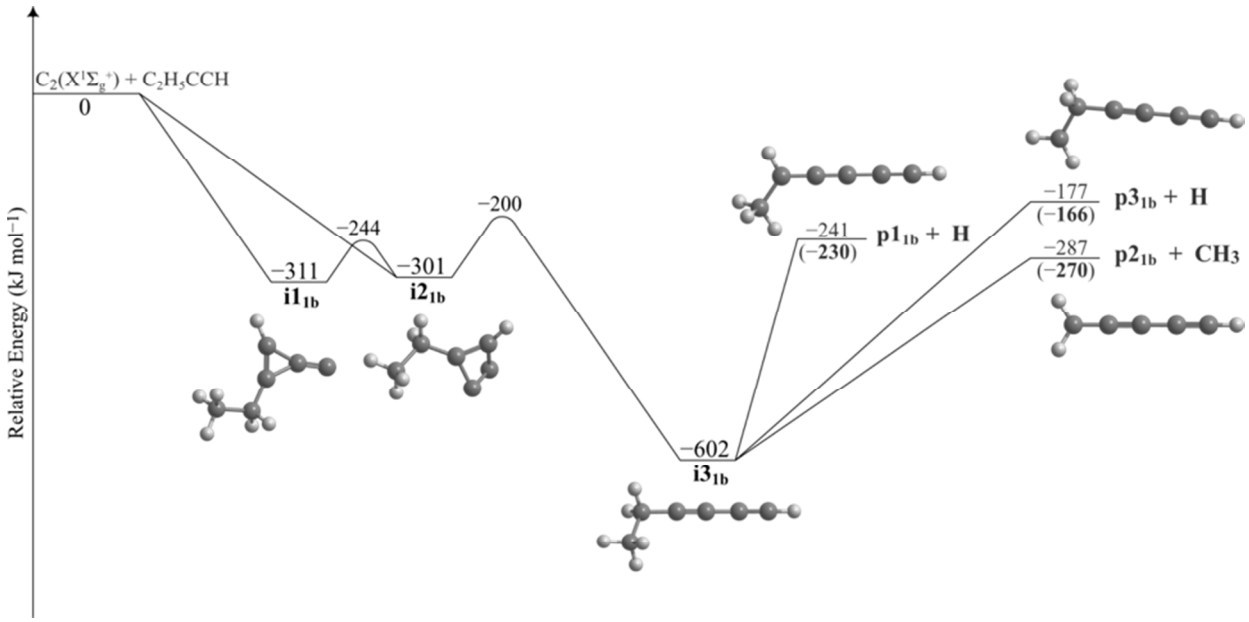

Figure 17. Schematic representation of the potential energy surface (PES) accessed by the reaction of dicarbon ($C_2(X^1\Sigma_g^+)$) plus 1-butyne (C_2H_5CCH (X^1A')) adopted from Parker et al.[68] All energies are relative to the separated reactants and given in kJ mol^{-1}. Plain and bold numbers show relative energies computed at the CCSD(T)/CBS(dt) and CCSD(T)/CBS(dtq) levels of theory respectively.

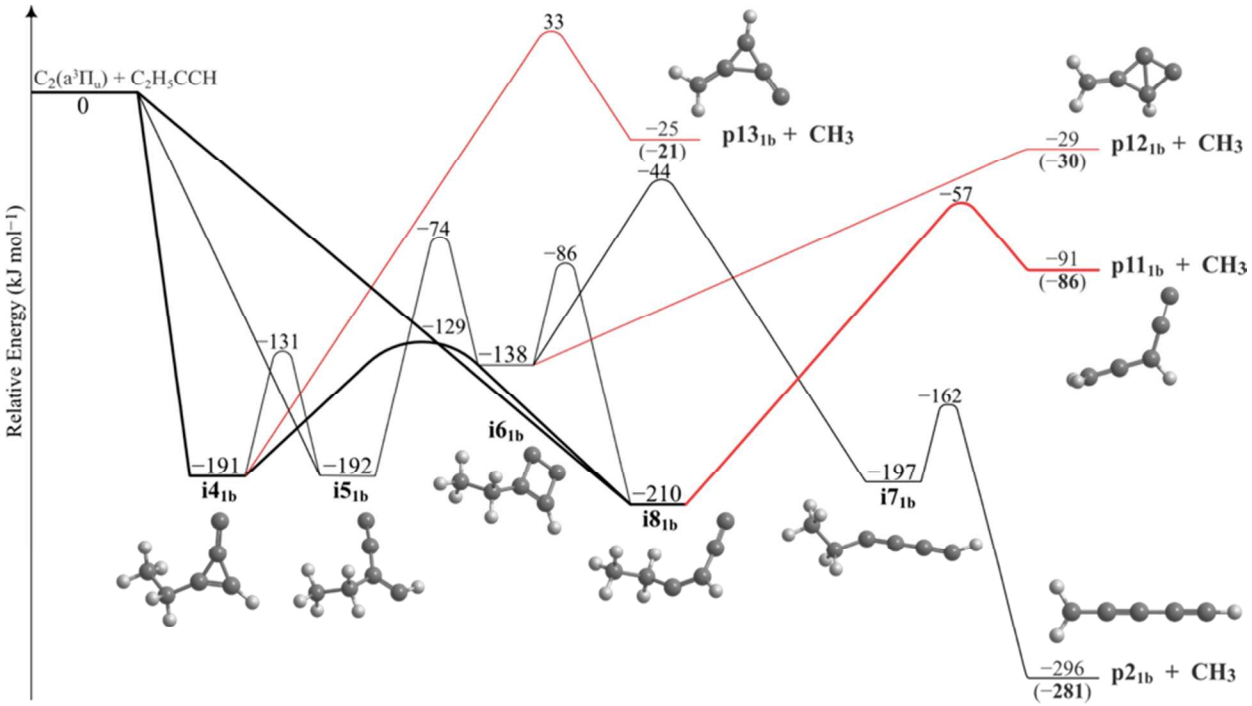

Figure 18. Schematic representation of the potential energy surface (PES) accessed by the reaction of dicarbon ($C_2(a^3\Pi_u)$) plus 1-butyne (C_2H_5CCH (X^1A')) adopted from Parker et al.[68] All energies are relative to the separated reactants and given in kJ mol^{-1}. Plain and bold numbers show relative energies computed at the CCSD(T)/CBS(dt) and CCSD(T)/CBS(dtq) levels of theory respectively. New pathways to C_5H_3 + CH_3 dissociation are shown in red and the dominant reaction channels are highlighted in bold.

Table 1. Peak velocities (v_p) and speed ratios (S) of the dicarbon (C_2), 1-butyne (C_2H_5CCH), methylacetylene (CH_3CCH), and d_3-methylacetylene (CD_3CCH) beams along with the corresponding collision energies (E_C) and center-of-mass angles (Θ_{CM}).

Beam	v_p (m s^{-1})	S	E_C (kJ mol^{-1})	Θ_{CM} (degree)
C_2 ($X^1\Sigma_g^+$/ $a^3\Pi_u$)	1567 ± 12	11.9 ± 0.6	23.2 ± 0.3	40.4 ± 0.4
CH_3CCH (X^1A_1)	800 ± 10	12.0 ± 0.4		
C_2 ($X^1\Sigma_g^+$/ $a^3\Pi_u$)	1579 ± 8	12.1 ± 0.6	24.0 ± 0.2	41.9 ± 0.4
CD_3CCH (X^1A_1)	790 ± 10	12.0 ± 0.4		
C_2 ($X^1\Sigma_g^+$/ $a^3\Pi_u$)	1596 ± 29	9.6 ± 0.9	26.2 ± 0.8	47.8 ± 0.7
C_2H_5CCH (X^1A')	782 ± 14	8.6 ± 0.5		

Table 2. Rotational temperatures and vibrational energy distribution in the two lowest electronic states of dicarbon.

Electronic State	Temperature (K)	$v = 0$ (%)	$v = 1$ (%)
Singlet ($X^1\Sigma_g^+$)	Total	81	19
	65	35	3
	1000	46	16
Triplet ($a^3\Pi_u$)	Total	74	26
	30	53	20
	300	21	6